Improving the Foundation Layers for Pavements

TECHNICAL REPORT:

Pavement Foundation Layer Reconstruction – Iowa I-35 Field Study



May 2016

Sponsored by
Federal Highway Administration (DTFH 61-06-H-00011 (Work Plan #18))
FHWA TPF-5(183): California, Iowa (lead state), Michigan, Pennsylvania, Wisconsin

National Concrete Pavement Technology Center
Tech Center

CENTER FOR CEER EARTHWORKS ENGINEERING RESEARCH
IOWA STATE UNIVERSITY
Institute for Transportation

About the National CP Tech Center

The mission of the National Concrete Pavement Technology (CP Tech) Center is to unite key transportation stakeholders around the central goal of advancing concrete pavement technology through research, tech transfer, and technology implementation.

About CEER

The mission of the Center for Earthworks Engineering Research (CEER) at Iowa State University is to be the nation's premier institution for developing fundamental knowledge of earth mechanics, and creating innovative technologies, sensors, and systems to enable rapid, high quality, environmentally friendly, and economical construction of roadways, aviation runways, railroad embankments, dams, structural foundations, fortifications constructed from earth materials, and related geotechnical applications.

Disclaimer Notice

The contents of this report reflect the views of the authors, who are responsible for the facts and the accuracy of the information presented herein. The opinions, findings and conclusions expressed in this publication are those of the authors and not necessarily those of the sponsors.

The sponsors assume no liability for the contents or use of the information contained in this document. This report does not constitute a standard, specification, or regulation.

The sponsors do not endorse products or manufacturers. Trademarks or manufacturers' names appear in this report only because they are considered essential to the objective of the document.

Iowa State University Non-Discrimination Statement

Iowa State University does not discriminate on the basis of race, color, age, ethnicity, religion, national origin, pregnancy, sexual orientation, gender identity, genetic information, sex, marital status, disability, or status as a U.S. veteran. Inquiries regarding non-discrimination policies may be directed to Office of Equal Opportunity, Title IX/ADA Coordinator, and Affirmative Action Officer, 3350 Beardshear Hall, Ames, Iowa 50011, 515-294-7612, email eooffice@iastate.edu.

Iowa Department of Transportation Statements

Federal and state laws prohibit employment and/or public accommodation discrimination on the basis of age, color, creed, disability, gender identity, national origin, pregnancy, race, religion, sex, sexual orientation or veteran's status. If you believe you have been discriminated against, please contact the Iowa Civil Rights Commission at 800-457-4416 or the Iowa Department of Transportation affirmative action officer. If you need accommodations because of a disability to access the Iowa Department of Transportation's services, contact the agency's affirmative action officer at 800-262-0003.

The preparation of this report was financed in part through funds provided by the Iowa Department of Transportation through its "Second Revised Agreement for the Management of Research Conducted by Iowa State University for the Iowa Department of Transportation" and its amendments.

The opinions, findings, and conclusions expressed in this publication are those of the authors and not necessarily those of the Iowa Department of Transportation or the U.S. Department of Transportation Federal Highway Administration.

Technical Report Documentation Page

1. Report No.	2. Government Accession No.	3. Recipient's Catalog No.
DTFH 61-06-H-00011 Work Plan 18		

4. Title and Subtitle	5. Report Date
Improving the Foundation Layers for Pavements: Pavement Foundation Layer Reconstruction – Iowa I-35 Field Study	May 2016
	6. Performing Organization Code

7. Author(s)	8. Performing Organization Report No.
David J. White, Pavana Vennapusa, Heath H. Gieselman, Yang Zhang, La Zhao, Jiake Zhang	InTrans Project 09-352

9. Performing Organization Name and Address	10. Work Unit No. (TRAIS)
National Concrete Pavement Technology Center and Center for Earthworks Engineering Research Iowa State University 2711 South Loop Drive, Suite 4700 Ames, IA 50010-8664	**11. Contract or Grant No.**

12. Sponsoring Organization Name and Address	13. Type of Report and Period Covered
Federal Highway Administration U.S. Department of Transportation 1200 New Jersey Avenue SE Washington, DC 20590	Technical Report
	14. Sponsoring Agency Code TPF-5(183)

15. Supplementary Notes

Visit www.cptechcenter.org or www.ceer.iastate.edu for color PDF files of this and other research reports.

16. Abstract

This technical project report is one of the field project reports developed as part of the TPF-5(183) and FHWA DTFH 61-06-H-00011:WO18 studies.

This report presents results and analysis from a field study conducted on interstate highway I-35 in Iowa. The project involved removal of the existing pavement and undercutting down to the new subgrade elevation, and placing 305 mm (12 in.) of special backfill on the subgrade as subgrade treatment and 152 mm (6 in.) of granular subbase. The new PCC pavement was 292 mm (11.5 in.) in thickness. The granular subbase material consisted of both virgin crushed limestone aggregate and recycled portland cement concrete material. The subbase layer construction process involved placing the material and compacting the layer with a smooth drum roller in a non-vibratory mode for a maximum of three passes followed by trimming process to trim the layer to the design grade. The main objective of this field study was to investigate the impacts of vibratory versus static mode of compaction and number of compaction passes on the granular subbase layer material properties such as material fines content, dry density, elastic modulus, California bearing ratio, modulus of subgrade reaction, and saturated hydraulic conductivity. Results from the field testing were analyzed using statistical t-tests to assess whether statistically significant differences exist between untrimmed and trimmed base layers and between low amplitude versus static compaction. The field test results indicated that the use of low amplitude vibration instead of the static mode of compaction can result in material degradation, as evidenced by increases in fines contents, but the resulting fines content were within the specified gradation limits. However, the trimming process resulted in much higher fines content, which in turn resulted in a denser and stiffer subbase layer but also decreased permeability values.

17. Key Words	18. Distribution Statement
concrete pavement—pavement foundation—quality assurance—quality control—recycled base—subbase—subgrade	No restrictions.

19. Security Classification (of this report)	20. Security Classification (of this page)	21. No. of Pages	22. Price
Unclassified.	Unclassified.	75	NA

Form DOT F 1700.7 (8-72) **Reproduction of completed page authorized**

IMPROVING THE FOUNDATION LAYERS FOR CONCRETE PAVEMENTS: PAVEMENT FOUNDATION LAYER RECONSTRUCTION – IOWA I-35 FIELD STUDY

Technical Report
May 2016

Research Team Members
Tom Cackler, David J. White, Jeffrey R. Roesler, Barry Christopher, Andrew Dawson, Heath Gieselman, and Pavana Vennapusa

Report Authors
David J. White, Pavana K. R. Vennapusa,
Heath H. Gieselman, Yang Zhang, La Zhao, Jiake Zhang
Iowa State University

Sponsored by
the Federal Highway Administration (FHWA)
DTFH61-06-H-00011 Work Plan 18
FHWA Pooled Fund Study TPF-5(183): California, Iowa (lead state), Michigan, Pennsylvania, Wisconsin

Preparation of this report was financed in part
through funds provided by the Iowa Department of Transportation
through its Research Management Agreement with the
Institute for Transportation
(InTrans Project 09-352)

National Concrete Pavement Technology Center and
Center for Earthworks Engineering Research
Iowa State University
2711 South Loop Drive, Suite 4700
Ames, IA 50010-8664
Phone: 515-294-8103
www.cptechcenter.org and www.ceer.iastate.edu

TABLE OF CONTENTS

ACKNOWLEDGMENTS ix
LIST OF SYMBOLS xi
EXECUTIVE SUMMARY xiii
CHAPTER 1. INTRODUCTION 1
CHAPTER 2. PROJECT INFORMATION 2
Project Background and Construction 2
Pavement Design Input Parameter Selection and Assumptions 5
CHAPTER 3. EXPERIMENTAL TEST METHODS 6
Laboratory Testing Methods and Data Analysis 6
In Situ Testing Methods 6
Real-Time Kinematic Global Positioning System 6
Nuclear Gauge 6
Zorn Light Weight Deflectometer 6
Dynamic Cone Penetrometer 7
Rapid Gas Permeameter Test 8
Static Plate Load Test 8
Roller-Integrated Compaction Measurements 9
Statistical Analysis 10
CHAPTER 4. EXPERIMENTAL TEST RESULTS 12
Description of Test Beds and In Situ Testing 12
TB1: Untrimmed Base (RPCC) 14
TB2: Trimmed base (RPCC) 26
TB3: Virgin Crushed Limestone and RPCC 34
Statistical Analysis Results 36
CHAPTER 5. SUMMARY AND CONCLUSIONS 44
REFERENCES 45
APPENDIX: STRESS-STRAIN CURVES FROM PLATE LOAD TESTS 47

LIST OF FIGURES

Figure 1. Moisture conditioning of aggregate after placement 3
Figure 2. Self-propelled smooth drum roller used by contractor (non-vibratory) 3
Figure 3. Total station for controlling leveling operations 4
Figure 4. Open graded base layer trimming operations 4
Figure 5. Trimble SPS-881 hand-held receiver (a), CAT CS683 smooth drum roller with CMV and MDP (b), Zorn LWD (c), gas permeability test (d), and static PLT (e) 7
Figure 6. E_{V1} and E_{V2} determination procedure from static PLT for subgrade and base materials 9
Figure 7. Locations of the test sections and measurement points obtained from GPS 13
Figure 8. TB1 and TB2: Test bed layout 14
Figure 9. TB1: Particle size distribution after low amplitude vibratory roller passes 15
Figure 10. TB1: K_{sat} and F_{200} after low amplitude vibratory roller passes 16
Figure 11. TB1: Moisture content and density after low amplitude vibratory roller passes 17
Figure 12. TB1: $E_{LWD\text{-}Z3}$ after low amplitude vibratory roller passes 17
Figure 13. TB1: DCP-CBR profiles after low amplitude vibratory roller passes 18
Figure 14. TB1: MDP* compaction curves after low amplitude vibratory roller passes 19
Figure 15. TB1: Particle size distributions after static compaction passes 20
Figure 16. TB1: K_{SAT} and F_{200} after static compaction passes 21
Figure 17. TB1: Moisture content and density after static compaction passes 22
Figure 18. TB1: $E_{LWD\text{-}Z3}$ after static compaction passes 22
Figure 19. TB1: DCP-CBR profiles after static compaction passes 23
Figure 20. TB1: MDP* compaction curves after static compaction passes 24
Figure 21. TB1: Comparison of in situ point measurements after low amplitude vibratory roller and static roller passes 25
Figure 22. TB2: K_{SAT} and F_{200} after low amplitude vibratory compaction roller passes 26
Figure 23. TB2: Moisture content and density after low amplitude vibratory compaction roller passes 27
Figure 24. TB2: $E_{LWD\text{-}Z3}$ after low amplitude vibratory compaction roller passes 27
Figure 25. TB2: DCP-CBR profiles after low amplitude vibratory compaction roller passes 28
Figure 26. TB2: K_{SAT} and F_{200} after static compaction roller passes 29
Figure 27. TB2: Moisture content and density after static compaction roller passes 30
Figure 28. TB2: $E_{LWD\text{-}Z3}$ after static compaction roller passes 30
Figure 29. TB2: MDP* compaction curves after static compaction roller passes 31
Figure 30. TB2: DCP-CBR profiles after static compaction roller passes 32
Figure 31. TB2: Comparison of average in situ point measurements after low amplitude vibratory and static compaction roller passes 33
Figure 32. TB3: MDP* compaction curves after low amplitude compaction roller passes 34
Figure 33. TB3: MDP* compaction curves after static compaction roller passes 35
Figure 34. TB3: Comparison of MDP*after low amplitude vibratory and static compaction roller passes 36
Figure 35. Box plots of DCP-CBR (UT indicates untrimmed; LA indicates low amplitude; TM indicates trimmed; ST indicates static) 37
Figure 36. Box plots of K_{sat} (UT indicates untrimmed; LA indicates low amplitude; TM indicates trimmed; ST indicates static) 38

Figure 37. Box plots of fines content, F_{200} (0-60 mm) (UT indicates untrimmed; LA indicates low amplitude; TM indicates trimmed; ST indicates static)....38
Figure 38. Box plots of moisture content, *w* (UT indicates untrimmed; LA indicates low amplitude; TM indicates trimmed; ST indicates static)....39
Figure 39. Box plots of density, γ_d (UT indicates untrimmed; LA indicates low amplitude; TM indicates trimmed; ST indicates static)....39
Figure 40. Box plots of $E_{LWD\text{-}Z3}$ (UT indicates untrimmed; LA indicates low amplitude; TM indicates trimmed; ST indicates static)....40
Figure 41. Box plots of MDP* (UT indicates untrimmed; LA indicates low amplitude; TM indicates trimmed; ST indicates static)....40
Figure 42. Box plots of E_{v1} and E_{v2} (UT indicates untrimmed; LA indicates low amplitude; TM indicates trimmed; ST indicates static)....41
Figure 43. TB1: Stress-strain curves after low amplitude vibratory compaction (0, 1)....47
Figure 44. TB1: Stress-strain curves after low amplitude vibratory compaction (2, 3)....48
Figure 45. TB1: Stress-strain curves after low amplitude vibratory compaction (6, 7)....49
Figure 46. TB1: Stress-strain curve after low amplitude vibratory compaction (8, 9)....50
Figure 47. TB1: Stress-strain curves after static compaction (1, 2)....51
Figure 48. TB1: Stress-strain curves after static compaction (3, 4)....52
Figure 49. TB1: Stress-strain curves after static compaction (5, 6)....53
Figure 50. TB1: Stress-strain curves after static compaction (7, 8)....54
Figure 51. TB2: Stress-strain curves after low amplitude vibratory compaction (0, 1)....55
Figure 52. TB2: Stress-strain curves after low amplitude vibratory compaction (2, 3)....56
Figure 53. TB2: Stress-strain curves after low amplitude vibratory compaction (4, 5)....57
Figure 54. TB2: Stress-strain curves after low amplitude vibratory compaction (6, 7)....58
Figure 55. TB2: Stress-strain curves after low amplitude vibratory compaction (8, 9)....59
Figure 56. TB2: Stress-strain curves after low amplitude vibratory compaction (1, 6)....60
Figure 57. TB2: Stress-strain curves after low amplitude vibratory compaction (7, 8)....61

LIST OF TABLES

Table 1. Summary of pavement thickness design input parameters/assumptions using the PCA 1984 method.....5
Table 2. Features of the vibratory smooth drum compaction roller 10
Table 3. Summary of t-test results to compare low amplitude (LA) and static (ST) compaction on untrimmed base (UT) 42
Table 4. Summary of t-test results to compare low amplitude compaction (LA) on untrimmed (UT) base and trimmed (TM) base.....43

ACKNOWLEDGMENTS

This research was conducted under Federal Highway Administration (FHWA) DTFH61-06-H-00011 Work Plan 18 and the FHWA Pooled Fund Study TPF-5(183), involving the following state departments of transportation:

- California
- Iowa (lead state)
- Michigan
- Pennsylvania
- Wisconsin

The authors would like to express their gratitude to the National Concrete Pavement Technology (CP Tech) Center, the FHWA, the Iowa Department of Transportation (DOT), and the other pooled fund state partners for their financial support and technical assistance.

Chris Brakee, Melissa Serio and several others with the Iowa Department of Transportation provided assistance in identifying the project, providing access to the project site, and obtaining project design information and specifications. We greatly appreciate his help.

Caterpillar, Inc. provided the CS-563 smooth drum roller used on the project, outfitted with compaction measurement and documentation systems.

We also thank the help of Stephen Quist and Bob Steffes of Iowa State University with laboratory and field testing. Christianna White provided comments and technical editing.

LIST OF SYMBOLS AND ACRONYMS

a	Plate radius
A′	Machine acceleration (m/s2)
B	Machine internal loss coefficients specific to a particular machine (kJ/s)
CBR	California bearing ratio
COV	Coefficient of variation
D_0	Deflection measured under the plate
DCP-CBR	California bearing ratio calculated from dynamic cone penetration values
DPI	Dynamic penetration index
E	Elastic modulus
E_{V1}	Initial load elastic modulus from plate load test
E_{V2}	Re-load elastic modulus from plate load test
$E_{LWD\text{-}Z3}$	Elastic modulus determined from 300 mm diameter plate light weight deflectometer
F	Shape factor
F_{200}	Percent passing No. 200 sieve
g	Acceleration due to gravity
G_o	Geometric factor, a constant based on the geometry of the device and test area
GPT	Rapid gas permeameter test device
k	Modulus of subgrade reaction
k_{comp}	Composite modulus of subgrade reaction
K_{gas}	Gas permeability
K_{rg}	Relative permeability to gas
K_{sat}	Saturated hydraulic conductivity from the rapid gas permeameter test device
k_1	Modulus of subgrade reaction
LA	Low-amplitude compaction
LWD	Lightweight deflectometer
m	Machine internal loss coefficients specific to a particular machine (kJ/m)
MDP	Machine drive power (kJ/s)
MDP*	Machine drive power-based measurement (manufacturer unitless scale of 1–150)
NG	Humboldt nuclear gauge
n_0 and n_1	number of measurements obtained from two different conditions
P_a	Atmospheric pressure
P_1	Absolute gas pressure on the soil surface
$P_{o(g)}$	Gauge pressure at the GPT orifice outlet
P_2	Atmospheric pressure
P_g	Gross power needed to move the smooth drum roller (kJ/s)
PLT	Plate load test
Q	Volumetric flow rate
r	Radius at the GPT outlet
s_0 and s_1	Standard deviation of the measurements obtained from two different conditions
S	Water saturation
S_e	Effective water saturation

S_p	Pooled standard deviation
S_r	Residual water saturation
ST	Static compaction
TM	Trimmed base
UT	Untrimmed base
v	Roller velocity (m/s)
w	Moisture content determined from Humboldt nuclear gauge
W	Roller weight (kN)
α	Slope angle (roller pitch from a sensor)
γ_d	Dry unit weight determined from Humboldt nuclear gauge
λ	Brooks-Corey pore size distribution index
μ	Statistical mean or average
μ_{water}	absolute viscosity of water (gm/cm-s)
η	Poisson's ratio
σ	Statistical standard deviation
σ_d	Applied stress
μ_{gas}	kinematic viscosity of the gas
ρ	density of water (g/sm^3)

EXECUTIVE SUMMARY

Quality foundation layers (the natural subgrade, subbase, and embankment) are essential to achieving excellent pavement performance. Unfortunately, many pavements in the United States still fail due to inadequate foundation layers. To address this problem, a research project, Improving the Foundation Layers for Pavements (FHWA DTFH 61-06-H-00011 WO #18; FHWA TPF-5(183)), was undertaken by Iowa State University (ISU) to identify, and provide guidance for implementing, best practices regarding foundation layer construction methods, material selection, in situ testing and evaluation, and performance-related designs and specifications. As part of the project, field studies were conducted in several in-service concrete pavements across the country that represented either premature failures or successful long-term pavements. A key aspect of each field study was to tie performance of the foundation layers to key engineering properties and pavement performance. In situ foundation layer performance data, as well as original construction data and maintenance/rehabilitation history data, were collected and geospatially and statistically analyzed to determine the effects of site-specific foundation layer construction methods, site evaluation, materials selection, design, treatments, and maintenance procedures on the performance of the foundation layers and of the related pavements. A technical report was prepared for each field study.

This report presents results and analysis from a field study conducted on interstate highway I-35 in Iowa. This project is located on I-35 in Hamilton County and involved reconstruction of the interstate highway from 1 mile north of IA 175 to 2.5 miles south of US20. The project involved removal of the existing pavement and undercutting down to the new subgrade elevation, and placing 305 mm (12 in.) of special backfill on the subgrade as subgrade treatment and 152 mm (6 in.) of granular subbase. The new PCC pavement was 292 mm (11.5 in.) in thickness. The special backfill material consisted of recycled material obtained from rubbilizing the existing pavement. The granular subbase material consisted of both virgin crushed limestone aggregate and recycled portland cement concrete material. The gradation requirements of the subbase material are from Section 4121 of the Iowa DOT standard specifications.

The Iowa State University (ISU) research team was present on site during construction of the granular subbase layer. The subbase layer construction process involved placing the material and compacting the layer with a smooth drum roller in a non-vibratory mode for a maximum of three passes followed by trimming process to trim the layer to the design grade. This placement and compaction process is in accordance with Section 2111 of the Iowa DOT standard specifications.

The main objective of this field study was to investigate the impacts of vibratory versus static mode of compaction and number of compaction passes on the granular subbase layer material properties such as material fines content, dry density, elastic modulus, California bearing ratio, modulus of subgrade reaction, and saturated hydraulic conductivity. Results from the field testing were analyzed using statistical t-tests to assess whether statistically significant differences exist between untrimmed and trimmed base layers and between low amplitude versus static compaction. Following are the key findings from analysis of the field test data:

- On the untrimmed granular subbase layer, CBR, γ_d, F_{200}, $E_{LWD\text{-}Z3}$, and E_{V1} showed statistically significant differences in the measurement values between low amplitude and static mode of compaction. The lane compacted with low amplitude mode resulted in higher values. There was no statistically significant difference in the *k*, K_{sat}, E_{v2}, and *w* measurements.
- On trimmed granular subbase layer, only K_{sat}, E_{v2}, and *w* measurements showed statistically significant differences between low amplitude and static compaction lanes. The lane compacted in static mode showed higher K_{sat} values. E_{v2} was higher in low amplitude compaction lane. There were no statistically significant differences in the remaining measurements between the static and low amplitude compaction lanes.
- For lanes compacted using low amplitude vibration, all measurements except CBR showed statistically significant differences between UT and TM base. γ_d, F_{200}, $E_{LWD\text{-}Z3}$, *k*, Ev_1 and E_{v2} were higher in TM base, while K_{sat} was lower in TM base.
- For lanes compacted in static mode, the t-test results show similar conclusions as the above case with low amplitude compaction. All measurements except CBR showed statistically significant differences between UT and TM base. γ_d, F_{200}, $E_{LWD\text{-}Z3}$, *k*, Ev_1 and E_{v2} were higher in TM base, while K_{sat} was lower in TM base.

These results indicate that the use of low amplitude vibration instead of the static mode of compaction can result in material degradation, as evidenced by increases in fines contents, but the resulting fines content were within the specified gradation limits. However, the trimming process resulted in much higher fines content, which in turn resulted in a denser and stiffer subbase layer but also decreased permeability values.

CHAPTER 1. INTRODUCTION

This report presents results and analysis from a field study conducted on interstate highway I-35 in Iowa. This project is located on I-35 in Hamilton County and involved reconstruction of the interstate highway from 1 mile north of IA 175 to 2.5 miles south of US20.

The project involved removal of the existing pavement and undercutting down to the new subgrade elevation, and placing 305 mm (12 in.) of special backfill on the subgrade as subgrade treatment and 152 mm (6 in.) of granular subbase. The new PCC pavement was 292 mm (11.5 in.) in thickness. The special backfill material consisted of recycled material obtained from rubbilizing the existing pavement. The granular subbase material consisted of both virgin crushed limestone aggregate and recycled portland cement concrete material. The gradation requirements of the subbase material was per Section 4121 of the Iowa DOT standard specifications.

The Iowa State University (ISU) research team was present on site during construction of the granular subbase layer. The subbase layer construction process involved placing the material and compacting the layer with a smooth drum roller in a non-vibratory mode for a maximum of three passes followed by trimming process to trim the layer to the design grade. This placement and compaction process is in accordance with Section 2111 of the Iowa DOT standard specifications.

The main objective of this field study was to investigate the assess the impacts of vibratory versus static mode of compaction and number of compaction passes on the granular subbase layer material properties such as material fines content, dry density, elastic modulus, California bearing ratio (CBR), modulus of subgrade reaction, and saturated hydraulic conductivity.

The ISU research team conducted field testing in three test beds (TB) that consisted of granular subbase layers before and after trimming. In each test bed, 1 to 9 roller passes were made in static and low amplitude vibration mode and followed by in situ point testing. A Caterpillar CS56 smooth drum vibratory roller equipped with machine drive power (MDP*) based roller integrated compaction monitoring system was used for compaction passes. In situ point testing involved nuclear gauge (NG) testing to determine material moisture content and dry density, dynamic cone penetrometer (DCP) to determine CBR, light weight deflectometer (LWD) to determine elastic modulus, static plate load test to determine modulus of subgrade reaction (k) value and elastic and re-load modulus, and air permeameter test (APT) to determine saturated hydraulic conductivity. The results are analyzed using statistical t-test analysis to assess if statistically significant differences exist between untrimmed and trimmed base layers, and low amplitude versus static compaction.

The findings from this report should be of significant interest to researchers, practitioners, and agencies who deal with design, construction, and maintenance aspects of PCC pavements. Results from this project provide one of several field project reports being developed as part of the TPF-5(183) and FHWA DTFH 61-06-H-00011:WO18 studies.

CHAPTER 2. PROJECT INFORMATION

This chapter presents brief background information on the project based on the project plans, design input parameters based on information obtained from the Iowa DOT pavement design engineer, and pictures taken during construction.

Project Background and Construction

This project is located on I-35 in Hamilton County and involved reconstruction of the interstate highway from 1 mile north of IA 175 to 2.5 miles south of US20. All ISU testing was performed on I-35 north bound lanes just north and south of the 270th St. overpass bridge near mile marker 139.

The project involved removal of the existing pavement and undercutting down to the new subgrade elevation, and placing 305 mm (12 in.) of special backfill on the subgrade as subgrade treatment and 152 mm (6 in.) of granular subbase. The new PCC pavement was 292 mm (11.5 in.) in thickness. The subbase layer construction process involved placing the material and compacting the layer with a smooth drum roller in a non-vibratory mode for a maximum of three passes followed by trimming process to trim the layer to the design grade. This placement and compaction process is in accordance with Section 2111 of the Iowa DOT standard specifications.

The ISU research team was present on site during construction of the granular subbase layer, and photographs are shown in Figure 1 to Figure 4. The subbase layer process involved placing the granular subbase layer and compacting the layer with a smooth drum roller in a non-vibratory mode for a maximum of three passes followed by trimming process to trim the layer to the design grade. This placement and compaction process is in accordance with Section 2111 of the Iowa DOT standard specifications.

Figure 1. Moisture conditioning of aggregate after placement

Figure 2. Self-propelled smooth drum roller used by contractor (non-vibratory)

Figure 3. Total station for controlling leveling operations

Figure 4. Open graded base layer trimming operations

Pavement Design Input Parameter Selection and Assumptions

A summary of pavement thickness design input parameters is provided in Table 1. A composite modulus of subgrade reaction, k_{comp} = 43 kPa/mm (160 pci), was determined by the Iowa DOT engineer following design guidelines in PCA (1984) as summarized in Table 1. The minimum design thickness was about 279 mm (11 in.) for the new pavement.

Table 1. Summary of pavement thickness design input parameters/assumptions using the PCA 1984 method

Parameter	Value
Surface Layer Design Assumptions	
Design period	40
Average daily traffic (ADT) volume	25,670 (2009) 76,669(2049)
Average daily truck traffic (ADTT) volume	14,733 (2049)
ADT annual growth	~3%
Doweled joints (yes/no)	Yes
Concrete shoulder (yes/no)	No
Concrete modulus of rupture	575
Load safety factor	1.2
Equivalent stresses (for single and tandem axles)	161 single, 154 tandem
Stress ratio factors (for single and tandem axles)	.280/.268
Erosion factors (for single and tandem axles)	2.40/2.62
Allowable load repetitions	Variable for each axle category
Lane distribution factor, *L*	1.0
Foundation Layer Design Assumptions	
Subgrade layer stiffness, *k* (pci)	125
Type of subbase (treated/untreated)	untreated
Subbase layer thickness	Variable (6 in. min, 8 in. avg)
Composite stiffness, k_{comp} (pci)	160
Pavement Thickness Design	
Calculated design thickness	11 in.

CHAPTER 3. EXPERIMENTAL TEST METHODS

This chapter summarizes the laboratory and in situ testing methods used in this study.

Laboratory Testing Methods and Data Analysis

Samples from the new open graded base layer were collected from the field and were carefully sealed and transported to the laboratory for testing. Particle-size analysis tests were performed in accordance with ASTM C136-06 *Standard test method for sieve analysis of fine and coarse aggregates*.

In Situ Testing Methods

The following in situ testing methods and procedures were used in this study: real-time kinematic (RTK) global positioning system (GPS); dynamic cone penetrometer (DCP); calibrated Humboldt nuclear gauge (NG); rapid gas permeameter device (GPT); static plate load test (PLT) setup with 300 mm diameter plate; and roller-integrated compaction monitoring measurements. Pictures of these test devices are shown in Figure 5.

Real-Time Kinematic Global Positioning System

A real-time kinematic GPS system (RTK-GPS) was used to obtain spatial coordinates (x, y, and z) of in situ test locations and tested pavement slabs. A Trimble SPS 881 receiver was used with base station correction provided from a Trimble SPS851 established on site Figure 3. According to the manufacturer, this survey system is capable of horizontal accuracies of < 10 mm and vertical accuracies of < 20 mm.

Nuclear Gauge

A calibrated Humboldt nuclear moisture-density gauge (NG) device was used to provide rapid measurements of soil dry unit weight (γ_d) and moisture content (w) in the base materials. Tests were performed following ASTM D6938-10 *Standard Test Method for In-Place Density and Water Content of Soil and Soil-Aggregate by Nuclear Methods (Shallow Depth)*. Measurements of w and γ_d were obtained at each test location and average values are reported.

Zorn Light Weight Deflectometer

Zorn LWD tests were performed on base and subbase layers to determine elastic modulus. The LWD was set up with a 300 mm diameter plate and a 71 cm drop height. The tests were performed following manufacturer recommendations (Zorn 2003), and the elastic modulus values were determined using Equation 1:

$$E = \frac{(1-\eta^2)\sigma_0 a}{D_0} \times F \quad (1)$$

where E = elastic modulus (MPa), D_0 = measured deflection under the plate (mm), η = Poisson's ratio (0.4), σ_0 = applied stress (MPa), r = radius of the plate (mm), F = shape factor depending on stress distribution (assumed as 8/3) (see Vennapusa and White 2009). The results are reported as $E_{LWD\text{-}Z3}$ where Z represents Zorn LWD and 3 represents 300 mm diameter plate.

Figure 5. Trimble SPS-881 hand-held receiver (a), CAT CS683 smooth drum roller with CMV and MDP (b), Zorn LWD (c), gas permeability test (d), and static PLT (e)

Dynamic Cone Penetrometer

DCP tests were performed in accordance with ASTM D6951-03 *Standard Test Method for Use of the Dynamic Cone Penetrometer in Shallow Pavement Applications* to determine dynamic penetration index (DPI) and calculate California bearing ratio (CBR) using Equation 2.

$$CBR = \frac{292}{DPI^{1.12}} \quad (2)$$

The DCP test results are presented in this report as CBR with depth profiles at a test location and as point values of average CBR of the subbase layer. The point data values represent the weighted average CBR within the granular subbase layer.

Rapid Gas Permeameter Test

The rapid gas permeameter test device (GPT) was used to determine saturated hydraulic conductivity of OGDC base and the existing subbase layers. GPT is a recently developed rapid permeability testing device that uses gas as a permeating fluid to determine the saturated hydraulic conductivity (K_{sat}) at a test location in situ (White et al. 2010a). Air was used as the permeating gas in this field study. The GPT consists of a self-contained pressurized gas system with a self-sealing base plate and a theoretical algorithm to rapidly determine the K_{sat}. The gas flow is controlled using a regulator and a precision orifice. The inlet pressure and flow rate values are recorded in the device and are used in K_{sat} calculations using Equation 3.

$$K_{sat} = \left[\frac{2\mu_{gas} Q P_1}{r\, G_o \left(P_1^{\,2} - P_2^{\,2} \right)} \right] \times \frac{\rho\, g}{\mu_{water} \left(1 - S_e\right)^2 \left(1 - S_e^{((2+\lambda)/\lambda)}\right)} \tag{3}$$

where K_{sat} = saturated hydraulic conductivity (cm/s); K_{gas} = gas permeability; K_{rg} = relative permeability to gas; μ_{gas} = kinematic viscosity of the gas (PaS); Q = volumetric flow rate (cm^3/s); P_1 = absolute gas pressure on the soil surface (Pa) $P_{o(g)}$ x 9.81 + 101325; $P_{o(g)}$ = gauge pressure at the orifice outlet (mm of H_20); P_2 = atmospheric pressure (Pa); r = radius at the outlet (4.45 cm); G_o= Geometric factor (constant based on geometry of the device and test area; White et al. 2007), S_e = effective water saturation [$S_e = (S - S_r)/(1-S_r)$]; λ = Brooks-Corey pore size distribution index; S_r = residual water saturation; S = water saturation; ρ = density of water (g/sm^3); g = acceleration due to gravity (cm/s^2); μ_{water} = absolute viscosity of water (gm/cm-s).

More details on the test device and K_{sat} calculation procedure are provided in White et al. (2007, 2010a). The degree of saturation (S) values were obtained from in situ dry unit weight and moisture content measurements. The S_r and λ parameters can be obtained by determining the soil-water retention properties (also known as soil water characteristic curves (SWCC) of the materials). Tests to determine the SWCC parameters can be time-consuming and require precise calibration of test equipment. As an alternative, empirical relationships from material gradation properties can be used (Zapata and Houston 2008). A summary of these relationships and the procedure to estimate S_r and λ parameters are summarized in White et al. (2010a). For the results presented in this report, λ = 0.98 and S_r = 12% were used for granular base material.

Static Plate Load Test

Static PLTs were conducted on the test sections by applying a static load on a 300 mm diameter plate against a 6.2 kN capacity reaction force. The applied load was measured using a 90-kN load cell and deformations were measured using three 50-mm LVDTs. The load and deformation readings were continuously recorded during the test using a data logger. The E_{V1} and E_{V2} values

were determined from Equation 1 using corresponding deflection values at 0.2 and 0.4 MPa contact stresses, respectively, as illustrated in Figure 6.

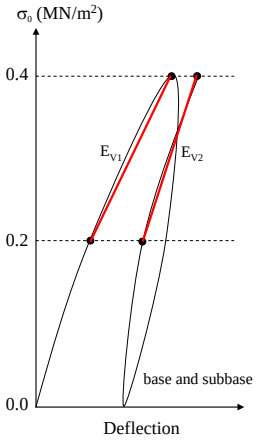

Figure 6. E_{V1} and E_{V2} determination procedure from static PLT for subgrade and base materials

Modulus of subgrade reaction was also determined from the PLT results by using Equation 4, where k_1 = modulus of subgrade reaction (kPa/mm), D_0 = measured deflection under the plate (mm) for 0.2 to 0.4 MPa applied stress range, and σ_0 = applied stress (kPa).

$$k_1 = \frac{\sigma_0}{D_0} \tag{4}$$

The PLT was performed using a 300 mm (12 in.) diameter plate, but the k_{comp} used in the AASHTO (1993) design guide is based on a 720 mm (30 in.) diameter plate. Therefore, the measured k_{comp} values were corrected for plate size using theoretical relationship (Equation 5) proposed by Terzaghi (Terzaghi and Peck 1967) for granular materials.

$$k_{comp} = k_1 \left[\frac{B + B_1}{2B} \right]^2 \tag{5}$$

where k_{comp} = modulus of subgrade reaction using a 762 mm (30 in.) diameter plate, k_1 = modulus of subgrade reaction using a 300 mm (12 in.) diameter plate, B_1 = 300 mm ; and B = 762 mm .

Roller-Integrated Compaction Measurements

The Caterpillar CS563 vibratory smooth drum roller used on the project was equipped with machine drive power (MDP) compaction monitoring technology. Brief descriptions of these

measurement values are provided below, and some key features of the roller are summarized in Table 2.

Table 2. Features of the vibratory smooth drum compaction roller

Parameter	Description
Drum Geometry	2.13 m width and 1.52 m diameter
Frequency (f)	30 Hz
Amplitude (a) Settings	Static, 0.90 mm (low amplitude), and 1.80 mm (high amplitude)
Compaction Measurement Value	Machine drive power based measurement value (shown as CCV in the output)
Display Software	AccuGrade
GPS coordinates	UTM Zone 15N (NAD83)
Output	Date/Time, Location (Northing/Easting/Elevation of left and right ends of the roller drum), Speed, CCV, CMV, Frequency, Amplitude, Direction (forward/backward), Vibration (On/Off)
Documentation	

MDP technology relates mechanical performance of the roller during compaction to the properties of the compacted soil. Detailed background information on the MDP system is provided in White et al. (2005). Controlled field studies documented by White and Thompson (2008), Thompson and White (2008), and Vennapusa et al. (2009) verified that MDP values are empirically related to soil compaction characteristics (i.e., density, stiffness, and strength). MDP is calculated using Equation 6.

$$MDP = P_g - Wv\left(Sin\alpha + \frac{A'}{g}\right) - \left(mv + b\right) \quad (6)$$

where MDP = machine drive power (kJ/s); P_g = gross power needed to move the machine (kJ/s); W = roller weight (kN); A′ = machine acceleration (m/s^2); g = acceleration of gravity (m/s^2); α = slope angle (roller pitch from a sensor); v = roller velocity (m/s); and m (kJ/m) and b (kJ/s) = machine internal loss coefficients specific to a particular machine (White et al. 2005).

MDP is a relative value referencing the material properties of the calibration surface, which is generally a hard compacted surface (MDP = 0 kJ/s). Positive MDP values therefore indicate material that is less compact than the calibration surface, while negative MDP values indicate material that is more compacted than the calibration surface (i.e., less roller drum sinkage). The MDP values obtained from the machine were recalculated to range between 1 and 150 according to the manufacturer (referred to as MDP* in this report).

Statistical Analysis

Student *t*-test analysis (Ott and Longnecker 2008) was conducted to assess differences between results obtained from sections with trimmed (TM) or untrimmed (UT) base material and results

obtained from sections with low amplitude compaction (LA) or static compaction (ST) using the following equations:

$$t = \frac{\mu_0 - \mu_1}{s_p \sqrt{\frac{1}{n_0} + \frac{1}{n_1}}} \tag{7}$$

where

$$s_p = \sqrt{\frac{(n_0 - 1) \times s_0^2 + (n_1 - 1) \times s_1^2}{n_0 + n_1 - 2}} \tag{8}$$

n_0 and n_1 = number of measurements obtained from the two sections being compared, respectively; S_p = pooled standard deviation; and s_0 and s_1 = standard deviation of measurements obtained the two sections being compared.

The observed *t*-values were compared with the minimum t-value for a one-tailed test with degree of freedom (df) = $n_0 + n_1 - 2$, for 95% confidence level (i.e., $\alpha = 0.05$). When comparing measurements from cracked or uncracked sections, if the *t*-values were greater than the minimum *t*-value, then it was concluded that there is sufficient evidence that the measurements were statistically different.

CHAPTER 4. EXPERIMENTAL TEST RESULTS

Description of Test Beds and In Situ Testing

A total of three test beds were tested in this field study. Test beds 1 and 2 (TB1 and TB2) consisted of RPCC material in the granular subbase and TB3 consisted of a mixture of RPCC and virgin crushed limestone material. The material was placed 1 to 2 days before testing. In TB1 and TB3, the material was not trimmed to grade (referred to as untrimmed base), while in TB2 it was trimmed to grade (referred to as trimmed base).

Each test bed was approximately 4.6 m (15 ft) wide x 122 to 214 m (400 to 700 ft) long. The test beds were divided into two side-by-side roller lanes that are about 2.3 m (7.5 ft) wide. Each lane was compacted either in static mode or in low amplitude vibratory mode using Caterpillar CS563 smooth drum roller. Each lane was then divided into 8 or 9 segments, in which each segment was compacted using roller passes ranging from 1 to 9. In situ tests were conducted in each segment after the compaction passes. The test bed layout along with test locations from GPS measurements are shown in Figure 7. A closer view of the test bed layout and test points from TB1 and TB2 is shown in Figure 8.

In situ testing in TB1 and TB2 involved LWD, GPT, MnDOT permeameter, PLT, NG, and DCP testing in each segment. In addition, bag samples of the subbase material were obtained from each test location from depths 0 to 60 mm and 60 to 100 mm below surface to perform gradation tests. Percent passing No. 200 sieve (F_{200}) were determined from each test location and a full gradation test was performed from one location in each segment. LWD and GPT tests, and F200 tests were performed at 3 locations from each segment, and all other tests MDP* values were obtained during the compaction passes from the roller. TB3 was also compacted and MDP* values were obtained but in situ testing was not performed after compaction due to rain at the time of testing.

In the following sections of the report, results from each test bed are presented separately for each measurement and is followed by results of statistical analysis assessing differences in the measurement values between trimmed vs. untrimmed base and static vs. low amplitude compaction test lanes.

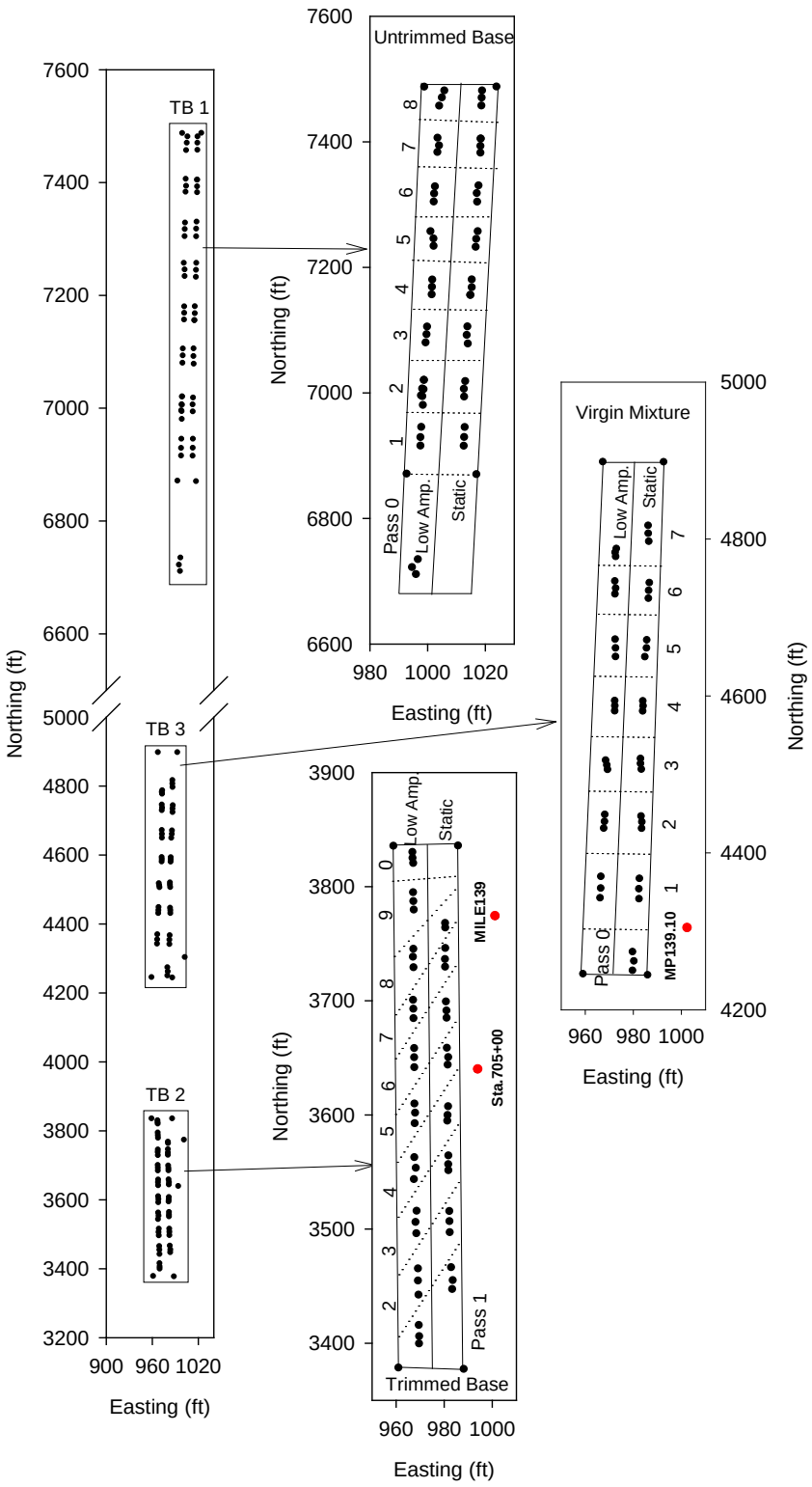

Figure 7. Locations of the test sections and measurement points obtained from GPS

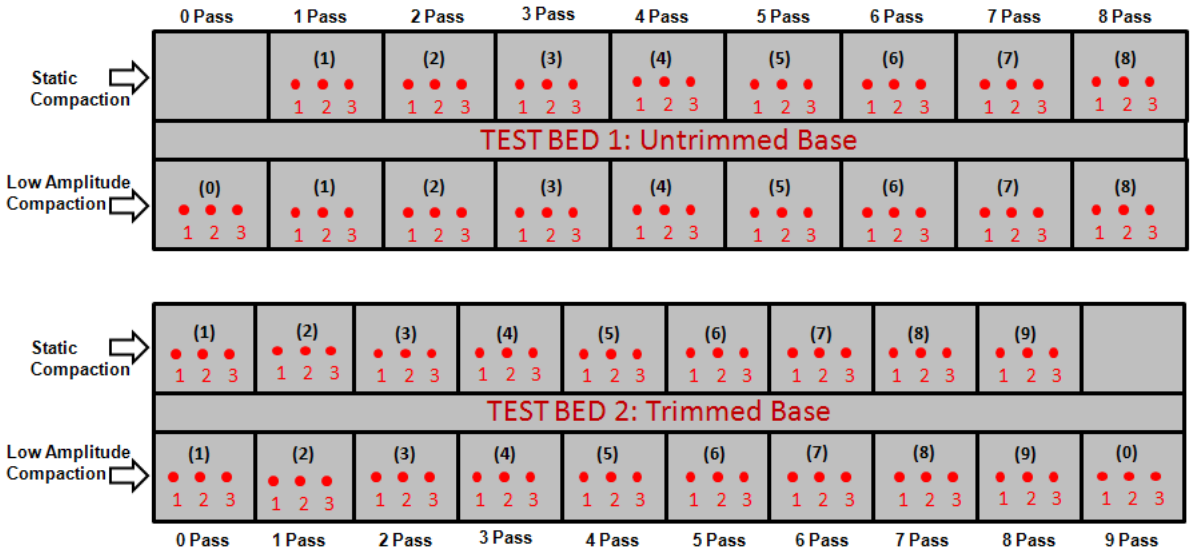

Figure 8. TB1 and TB2: Test bed layout

TB1: Untrimmed Base (RPCC)

TB1 consisted of two lanes, one compacted in static mode and one in low amplitude vibration mode. Results of the two lanes are presented separately in the following.

Particle size distribution curves from one sample obtained in each segment compacted to passes 1 to 8 are shown in Figure 9. K_{sat} and F_{200} from 0 to 60 and 60 to 100 mm depths for each segment are shown in Figure 10. Moisture and dry density measurements from NG are presented in Figure 11. Elastic modulus measurements from LWD test are presented in Figure 12. DCP-CBR profiles are shown in Figure 13. MDP* measurements are presented in Figure 14. The results from the static compaction lane are presented in Figure 15 to Figure 20.

All the measurements are compared in plots showing each measurement value versus compaction passes in Figure 21. The results indicated that the moduli values from PLT and LWD, dry density values and CBR values were all slightly higher in the lane compacted in vibratory mode. F_{200} values were generally higher in the low amplitude lane, although all were within the maximum allowed F_{200} of 6% for the granular subbase material. MDP* values were higher in the static lane although it must be noted that MDP* values are influenced by the compaction mode.

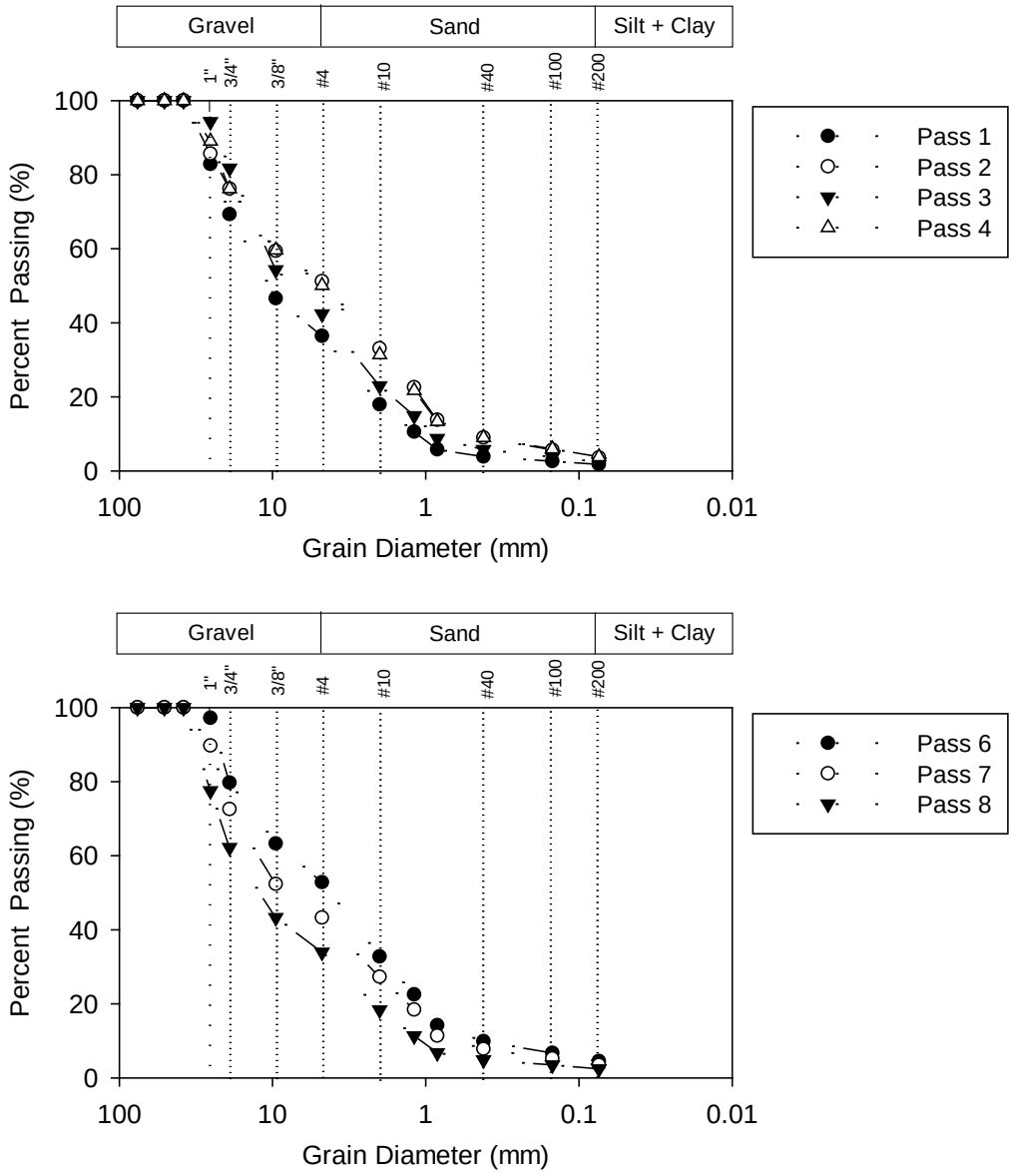

Figure 9. TB1: Particle size distribution after low amplitude vibratory roller passes

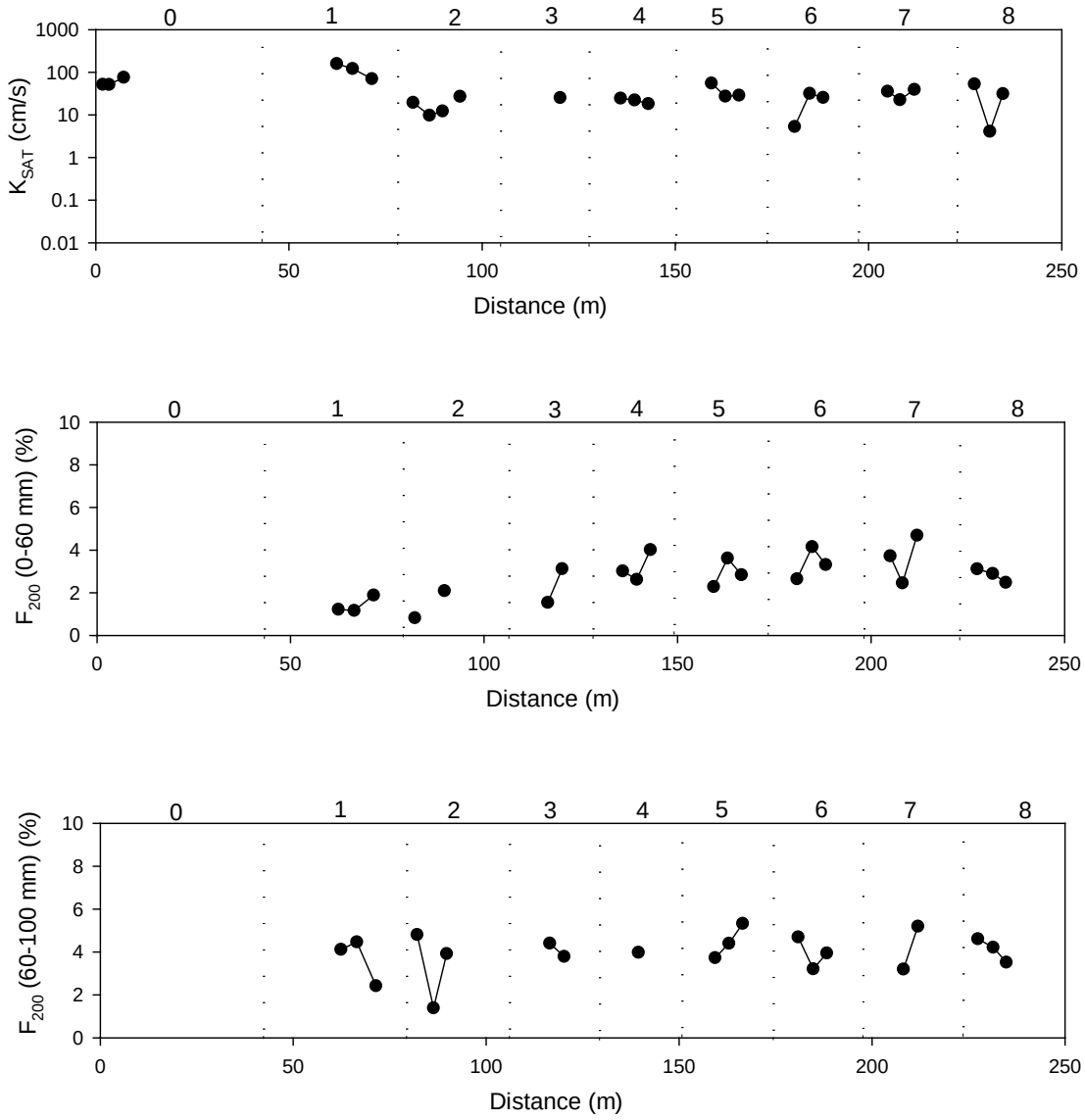

Figure 10. TB1: K_{sat} and F_{200} after low amplitude vibratory roller passes

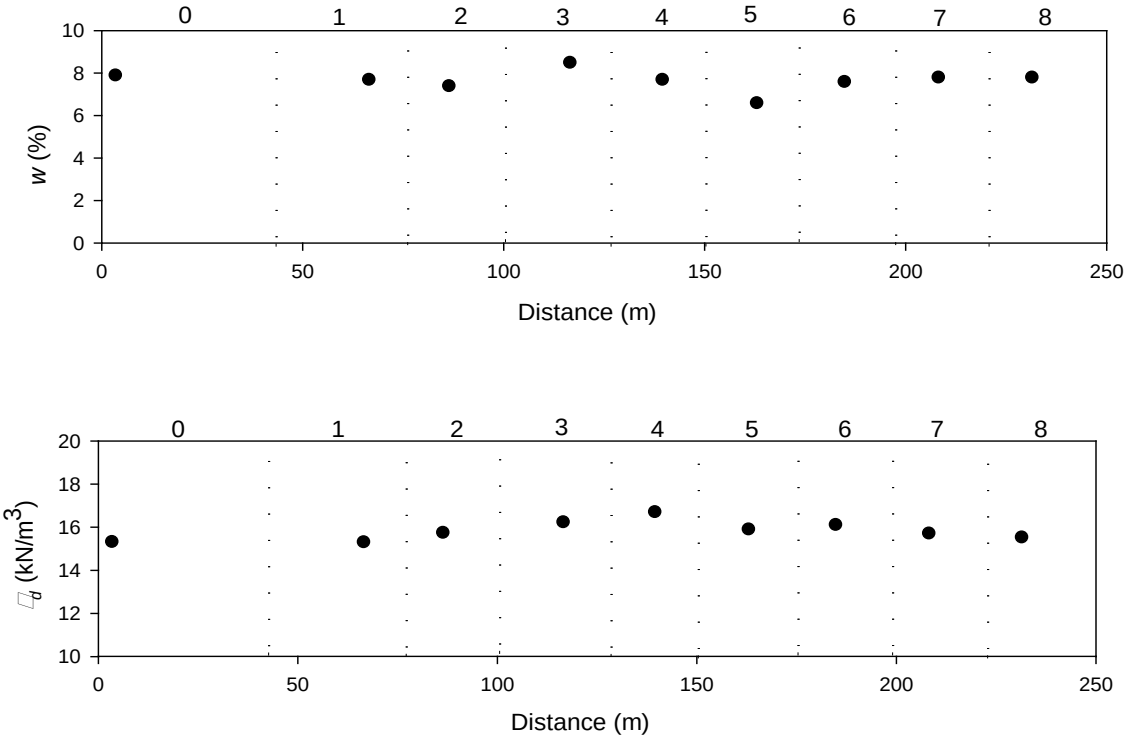

Figure 11. TB1: Moisture content and density after low amplitude vibratory roller passes

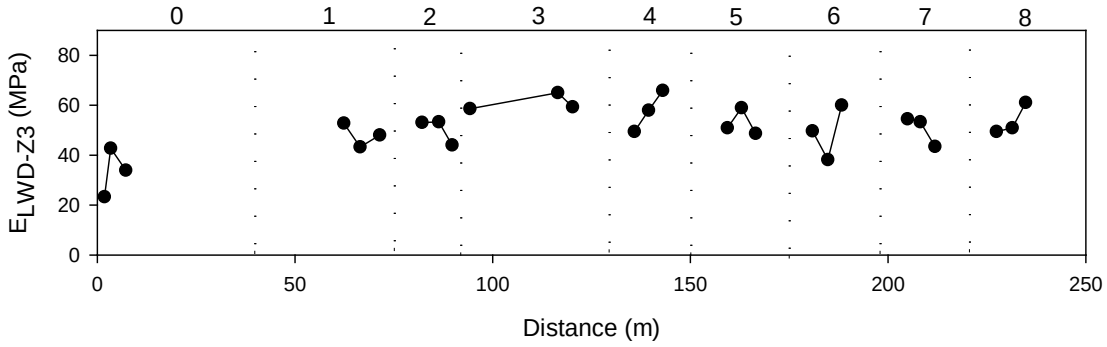

Figure 12. TB1: $E_{LWD\text{-}Z3}$ after low amplitude vibratory roller passes

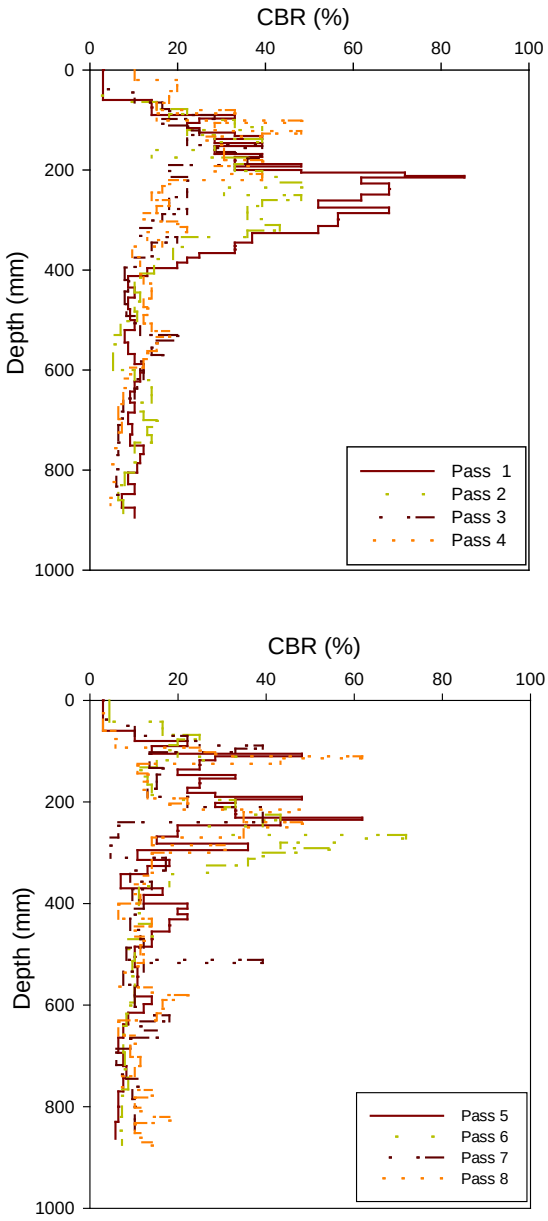

Figure 13. TB1: DCP-CBR profiles after low amplitude vibratory roller passes

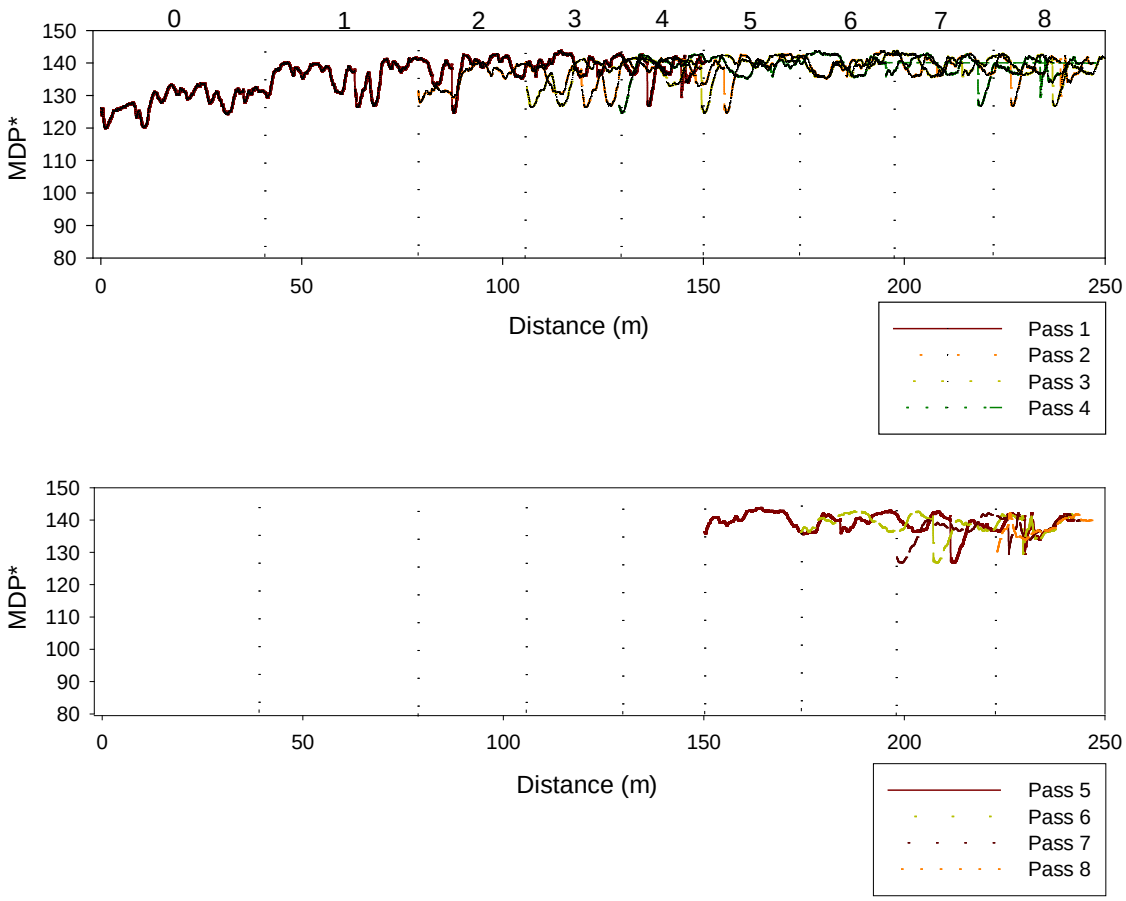

Figure 14. TB1: MDP* compaction curves after low amplitude vibratory roller passes

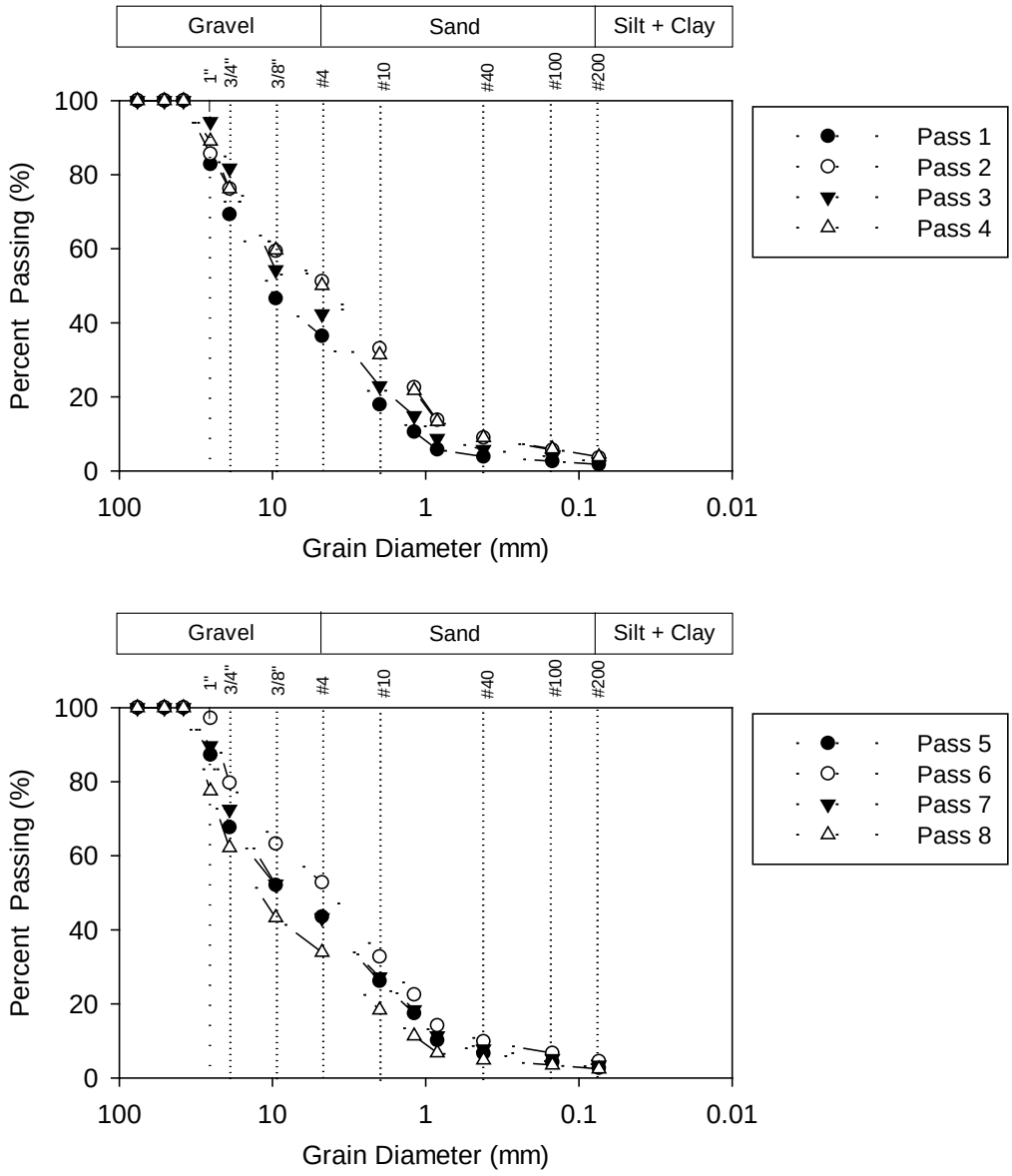

Figure 15. TB1: Particle size distributions after static compaction passes

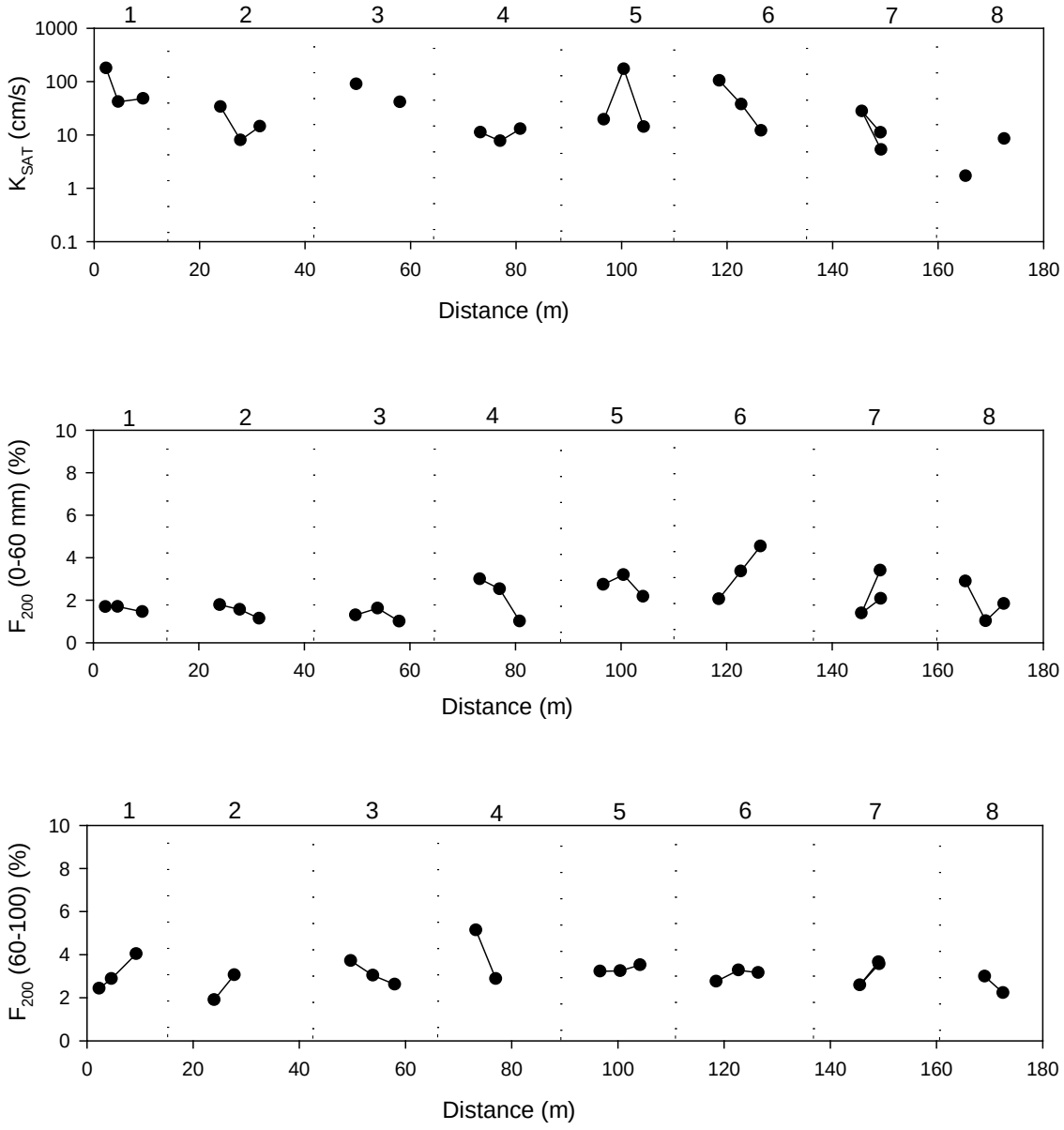

Figure 16. TB1: K_{SAT} and F_{200} after static compaction passes

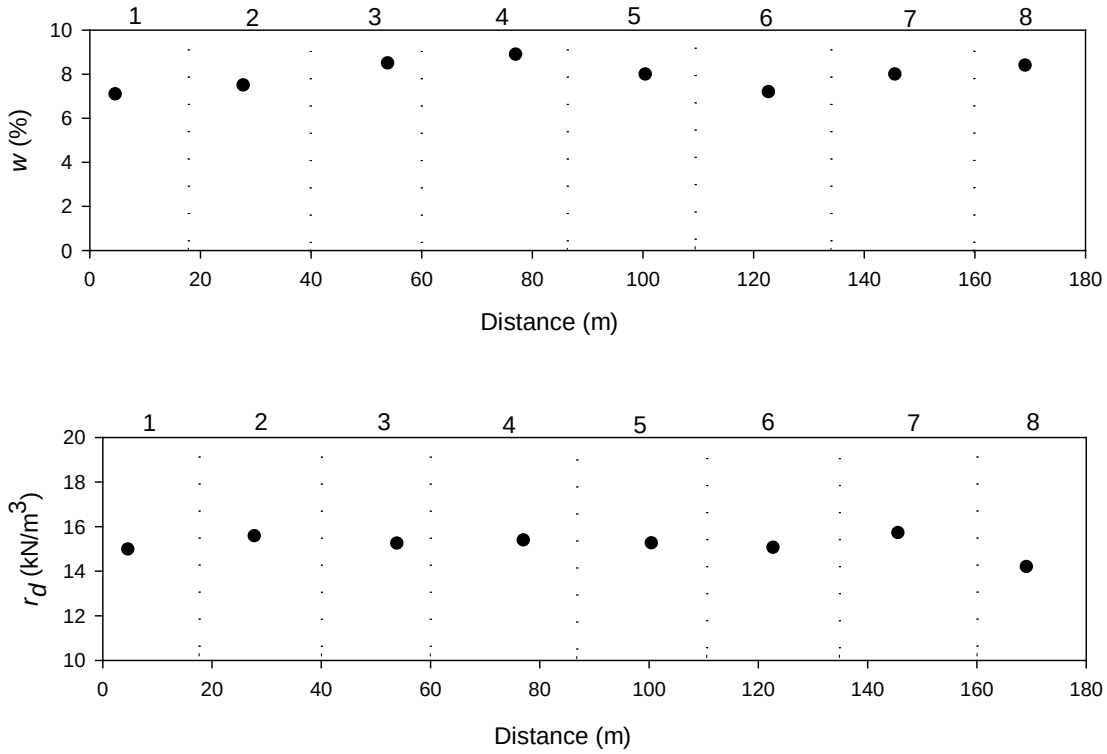

Figure 17. TB1: Moisture content and density after static compaction passes

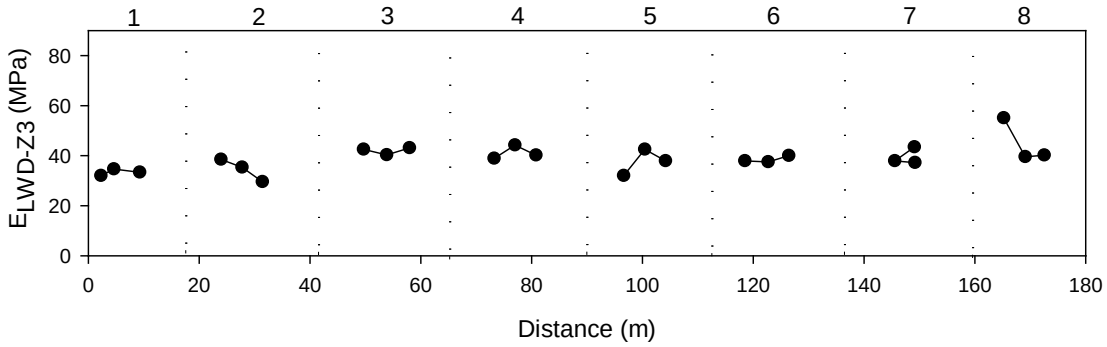

Figure 18. TB1: $E_{LWD\text{-}Z3}$ after static compaction passes

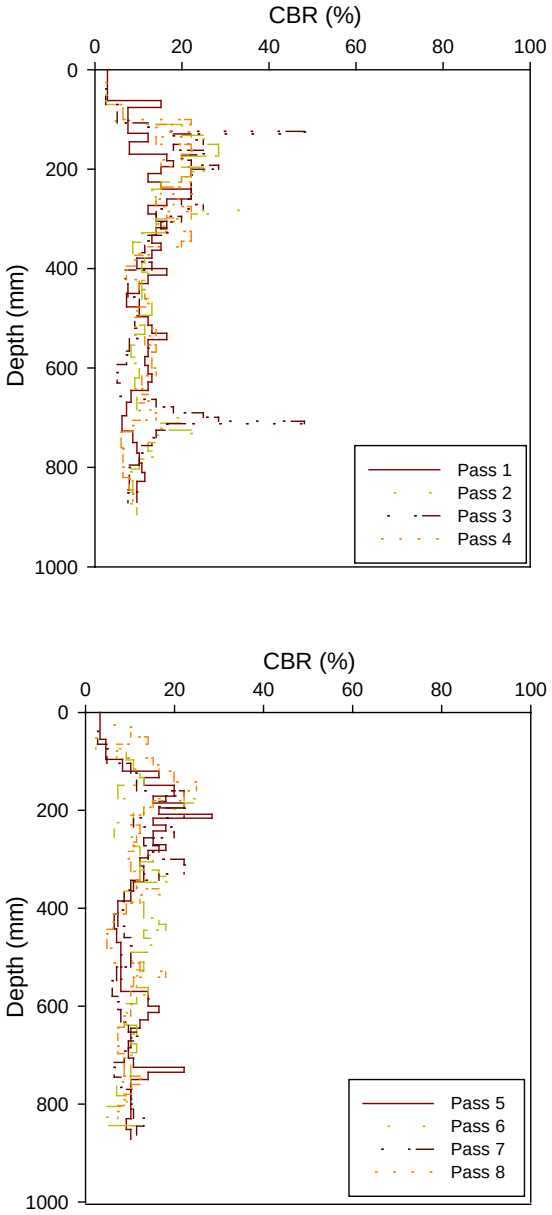

Figure 19. TB1: DCP-CBR profiles after static compaction passes

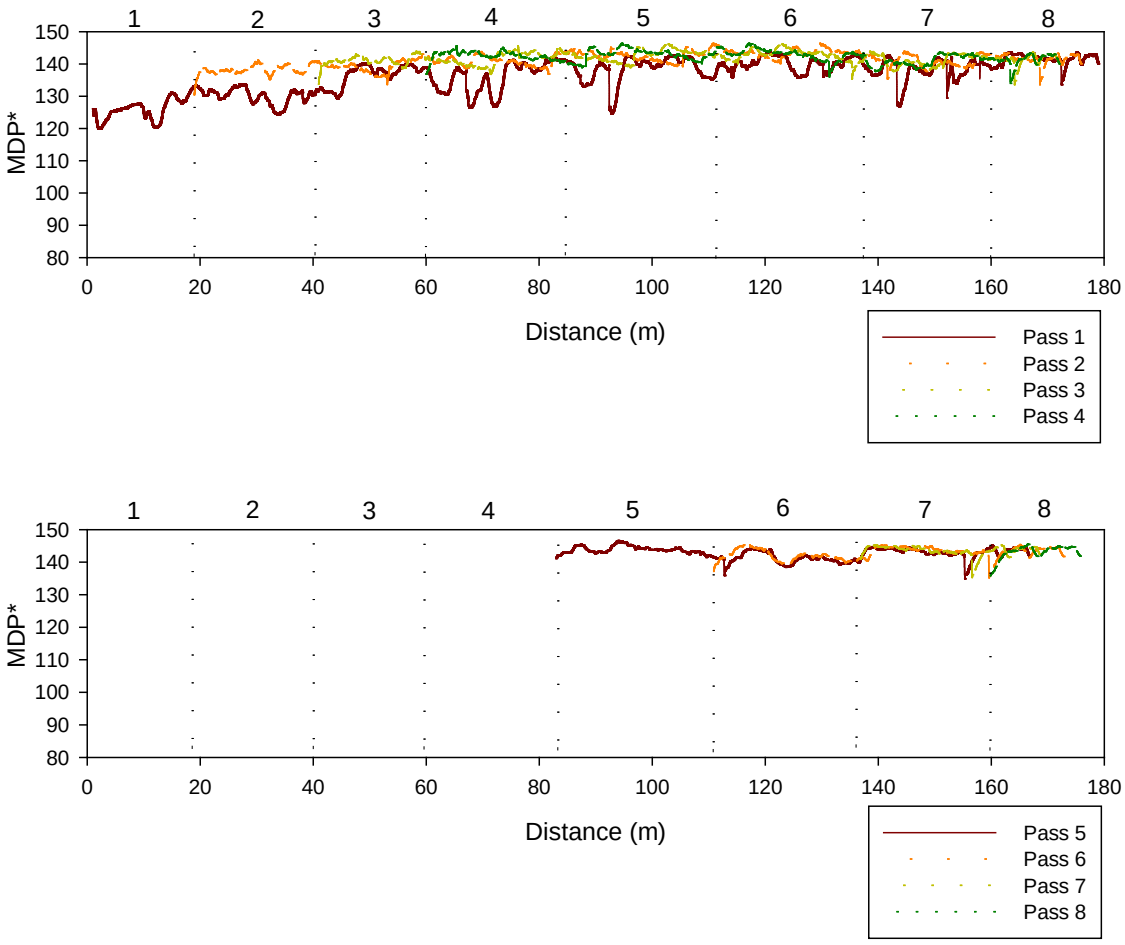

Figure 20. TB1: MDP* compaction curves after static compaction passes

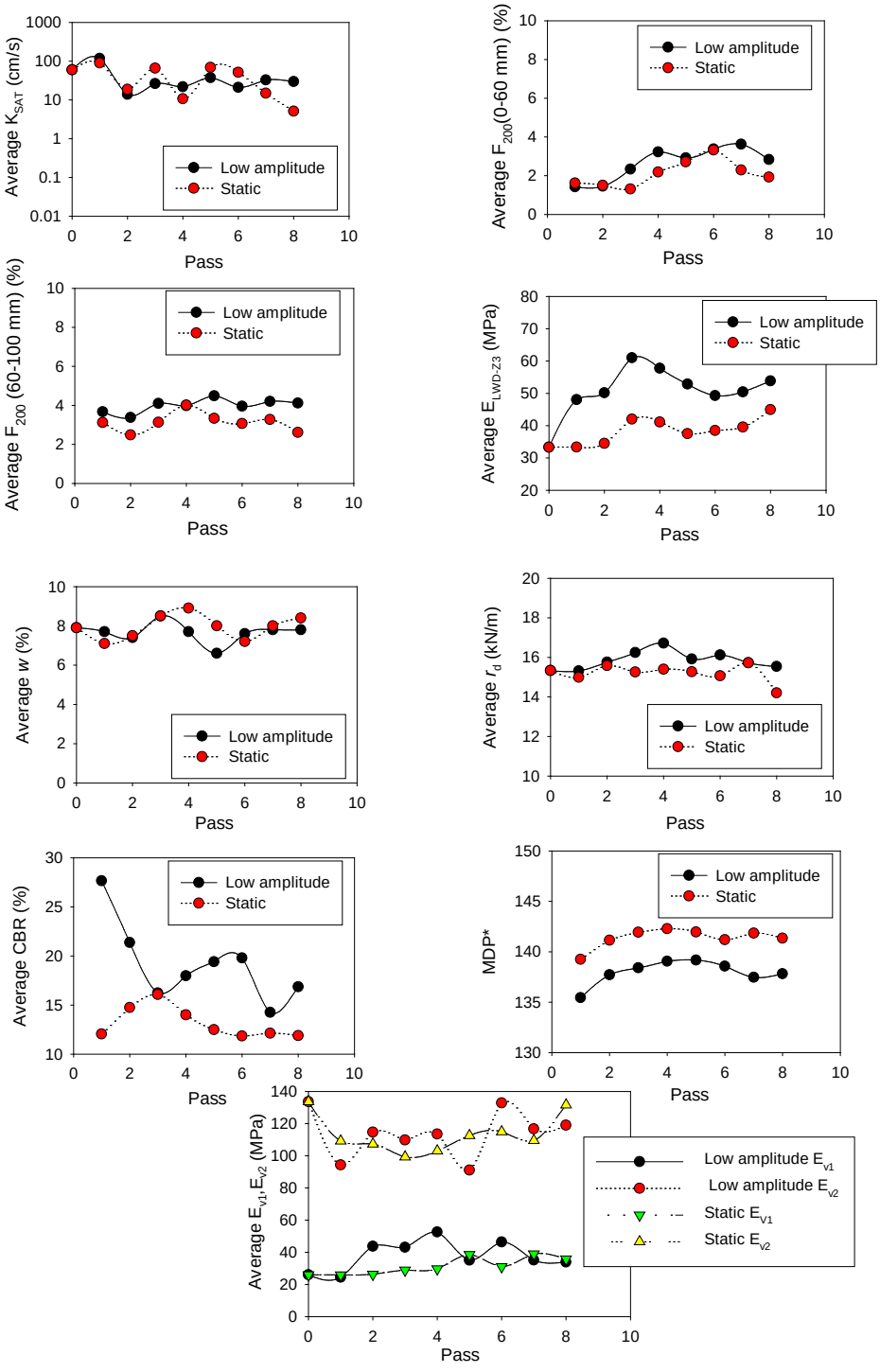

Figure 21. TB1: Comparison of in situ point measurements after low amplitude vibratory roller and static roller passes

TB2: Trimmed base (RPCC)

TB2 consisted of two lanes, one compacted in static mode and one in low amplitude vibration mode. Testing was conducted after compaction and trimming operations were performed by the contractor. Results of the two lanes are presented separately in the following.

Results from the lane compacted using low amplitude vibration are presented in Figure 22 to Figure 25 and the results from the static compaction lane are presented in Figure 26 to Figure 30. No significant differences were observed between measurements from the two lanes. Statistical analysis is performed on this data to assess statistically significance and is presented in the following sections of the report.

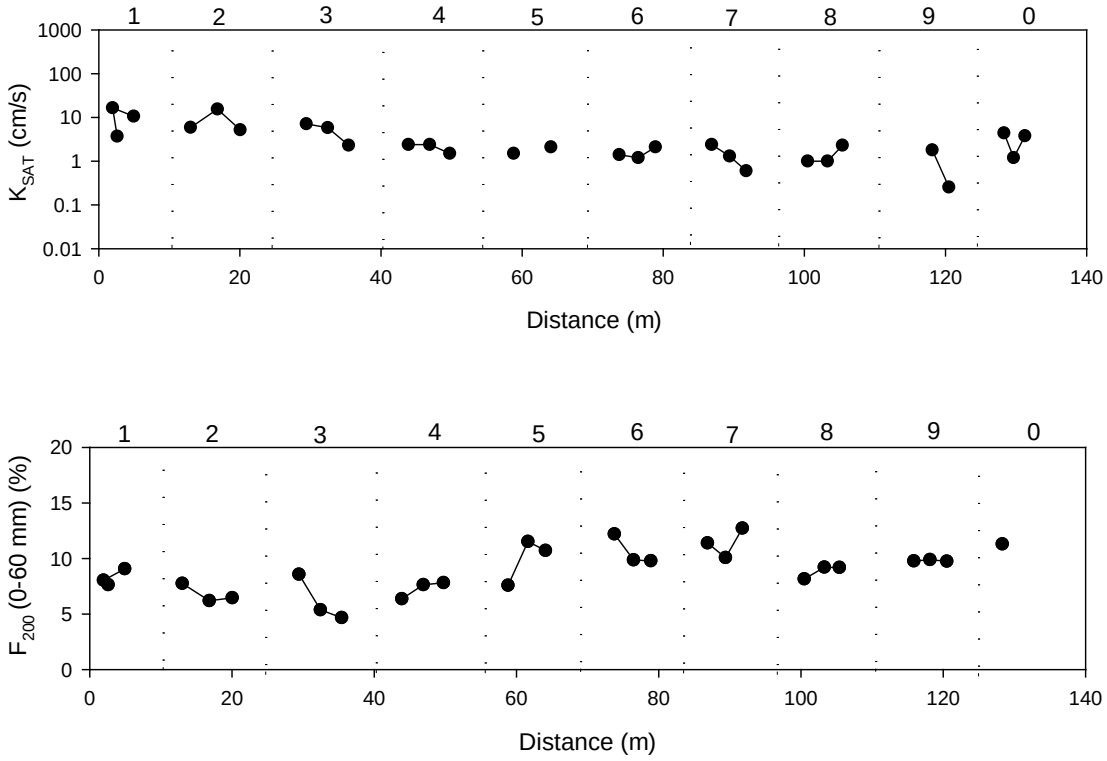

Figure 22. TB2: K_{SAT} and F_{200} after low amplitude vibratory compaction roller passes

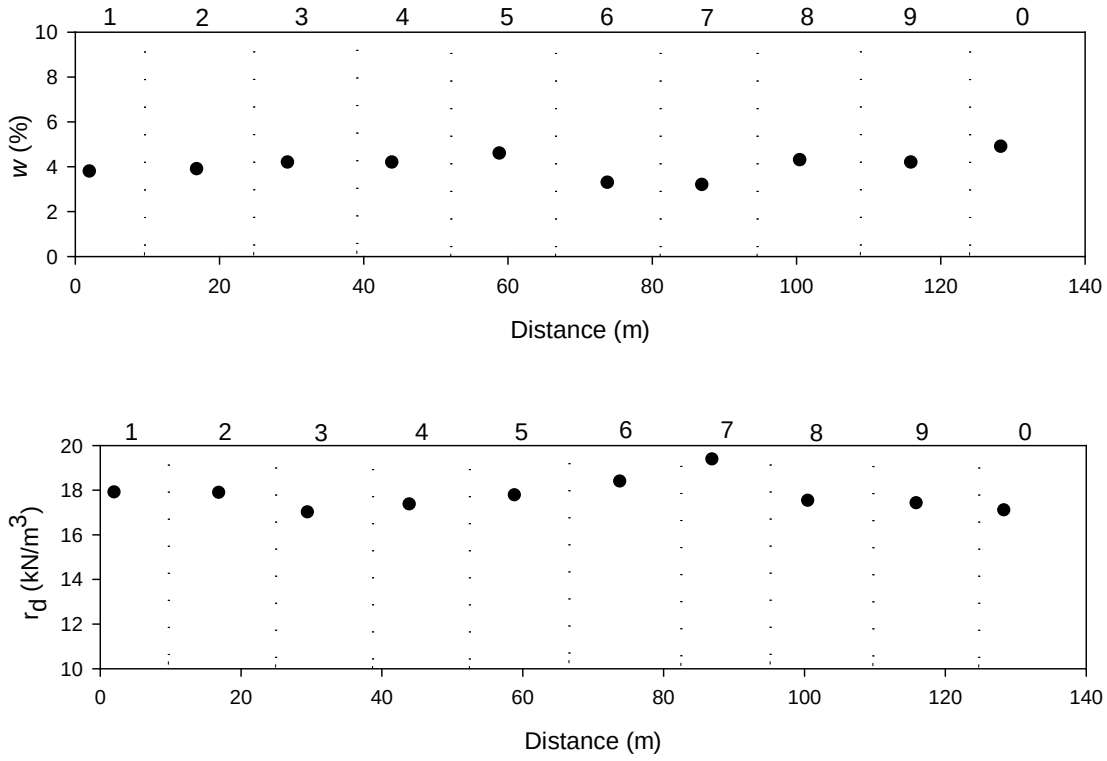

Figure 23. TB2: Moisture content and density after low amplitude vibratory compaction roller passes

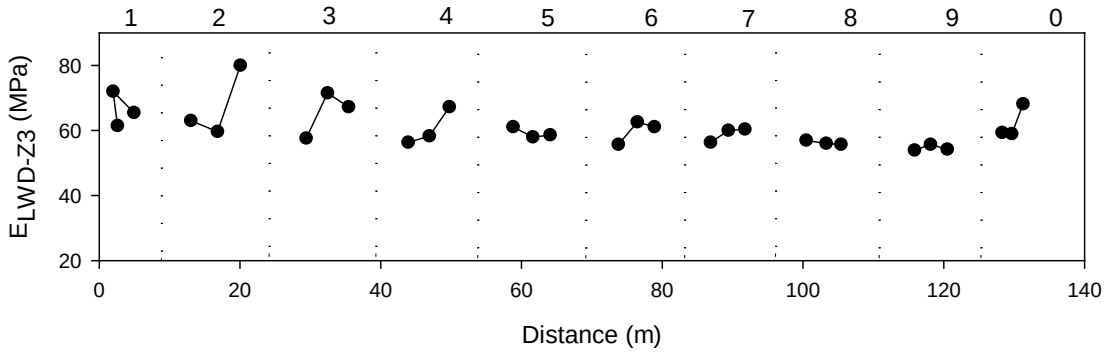

Figure 24. TB2: $E_{LWD\text{-}Z3}$ after low amplitude vibratory compaction roller passes

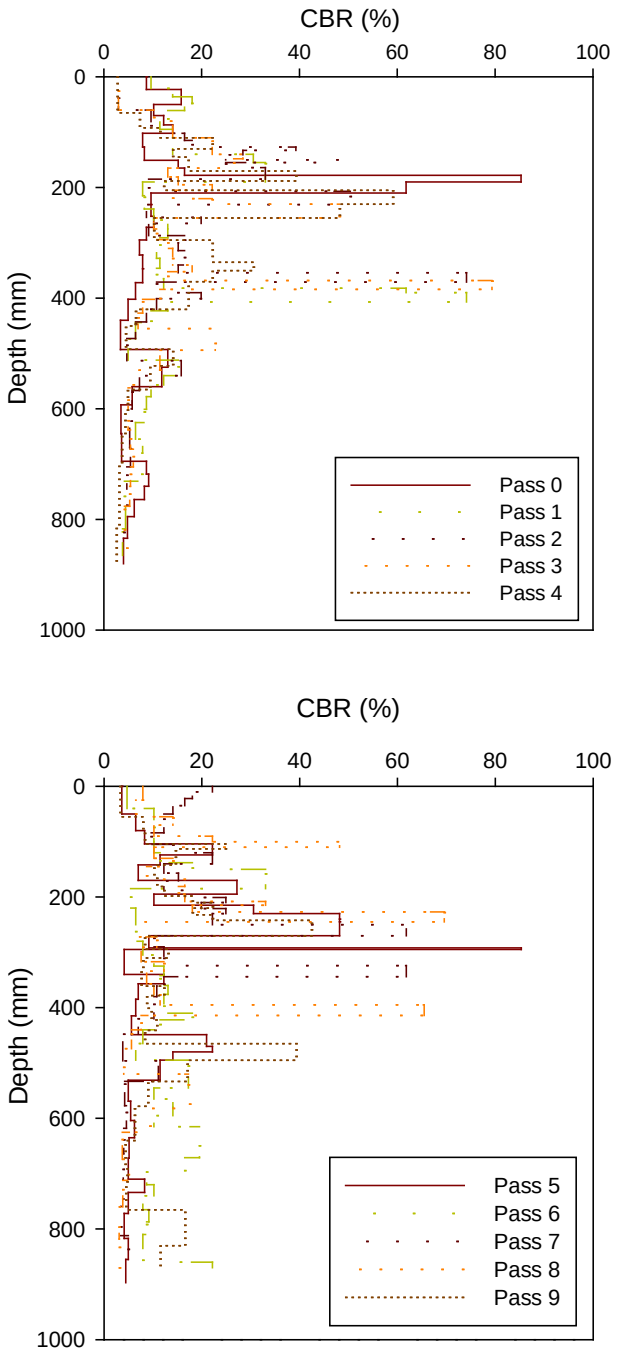

Figure 25. TB2: DCP-CBR profiles after low amplitude vibratory compaction roller passes

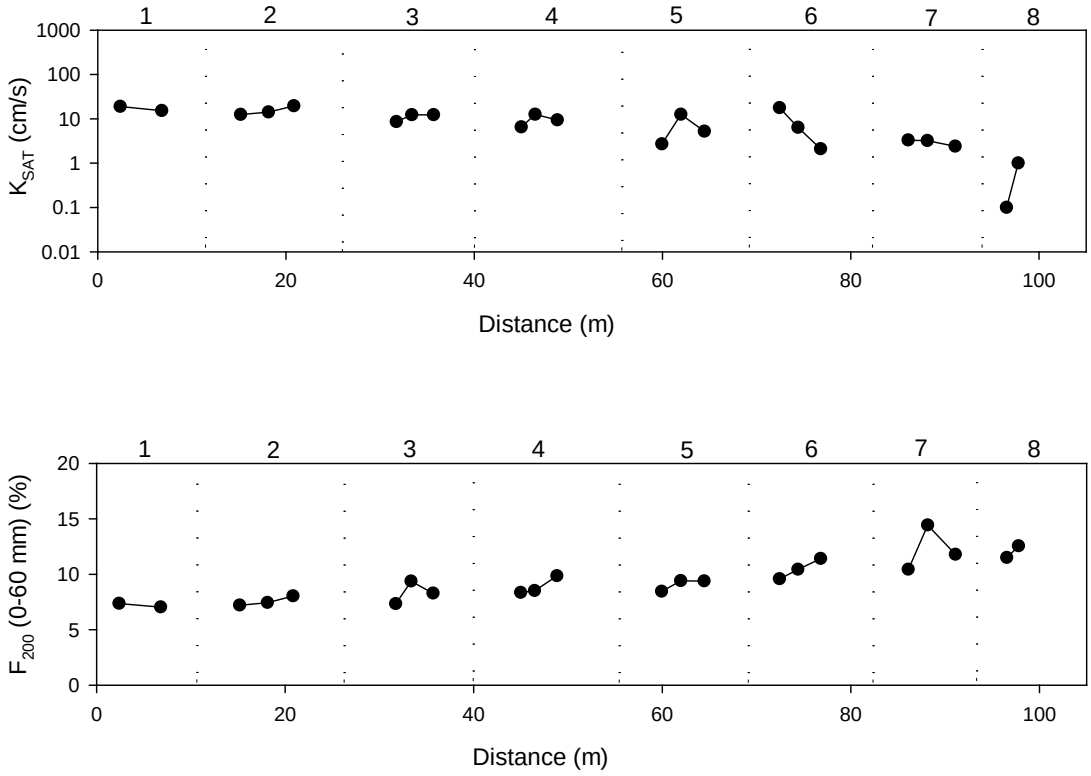

Figure 26. TB2: K_{SAT} and F_{200} after static compaction roller passes

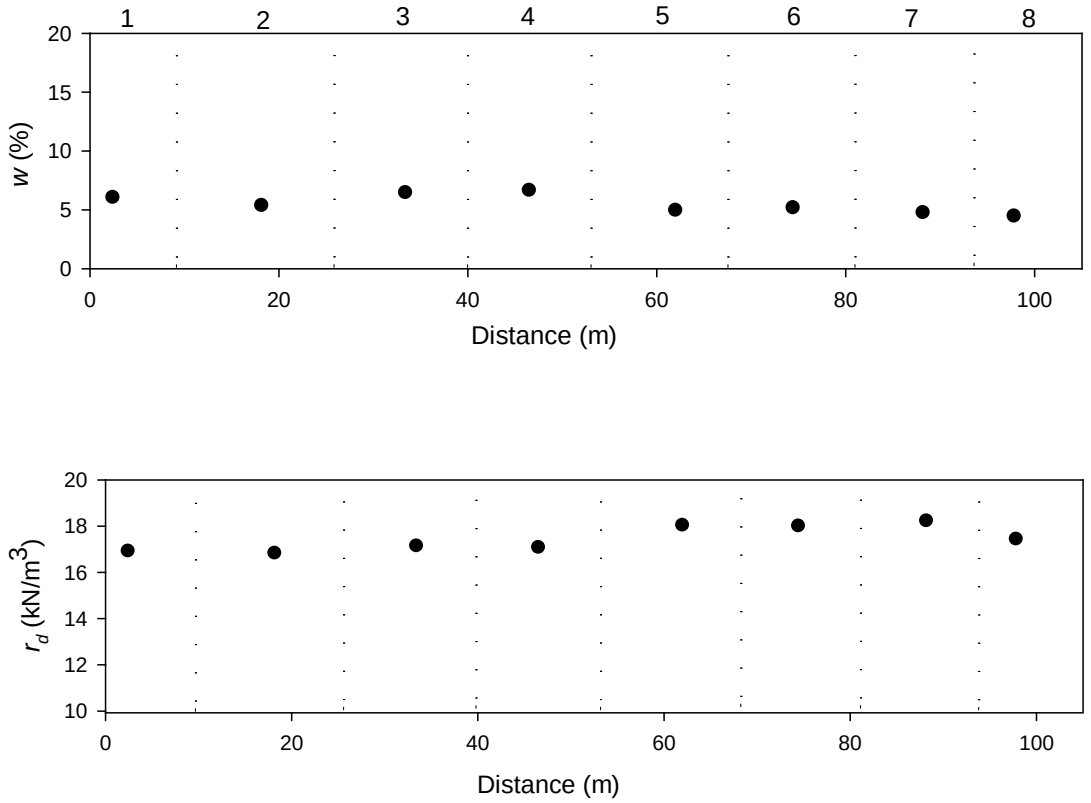

Figure 27. TB2: Moisture content and density after static compaction roller passes

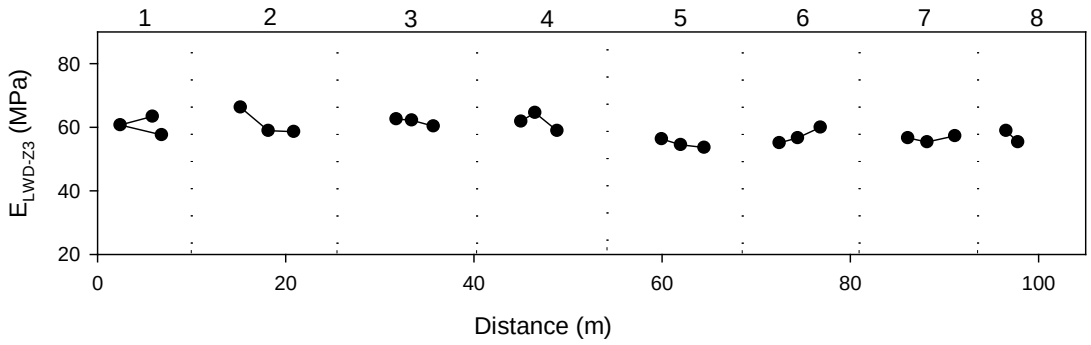

Figure 28. TB2: $E_{LWD\text{-}Z3}$ after static compaction roller passes

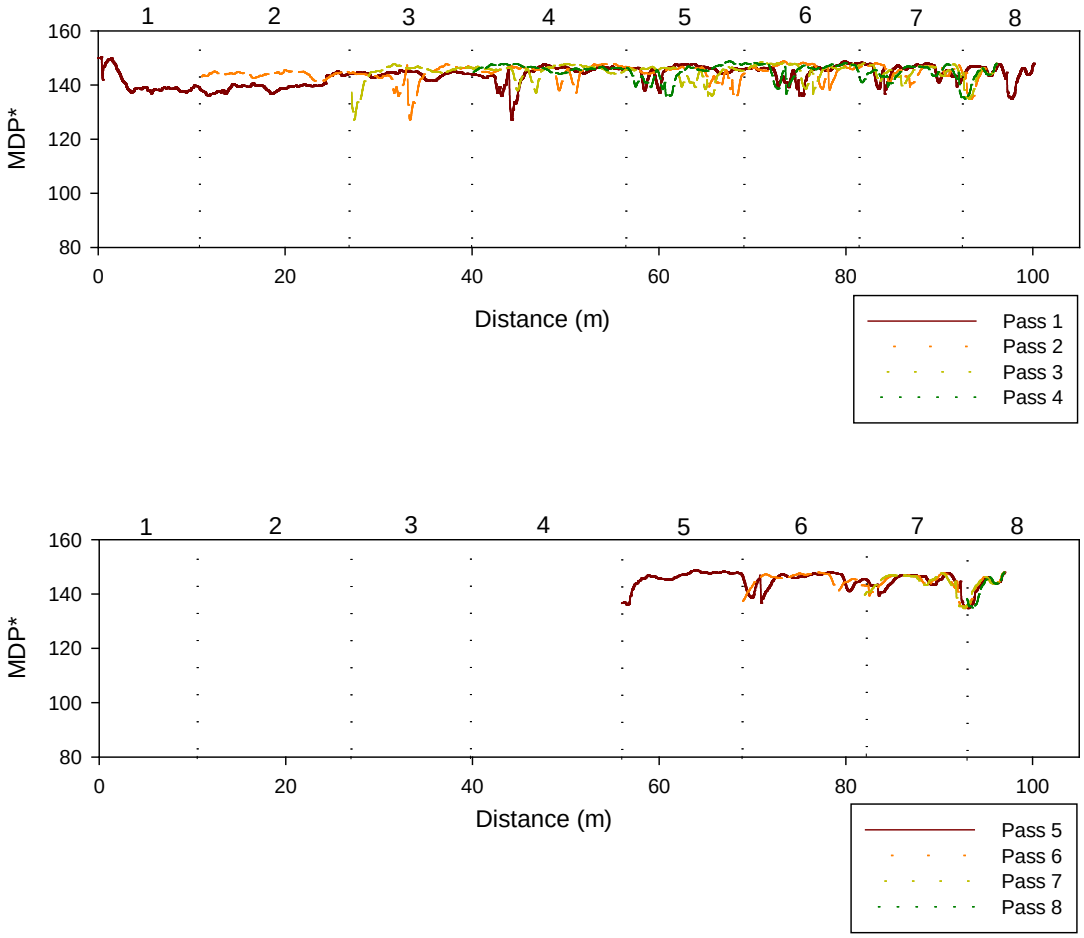

Figure 29. TB2: MDP* compaction curves after static compaction roller passes

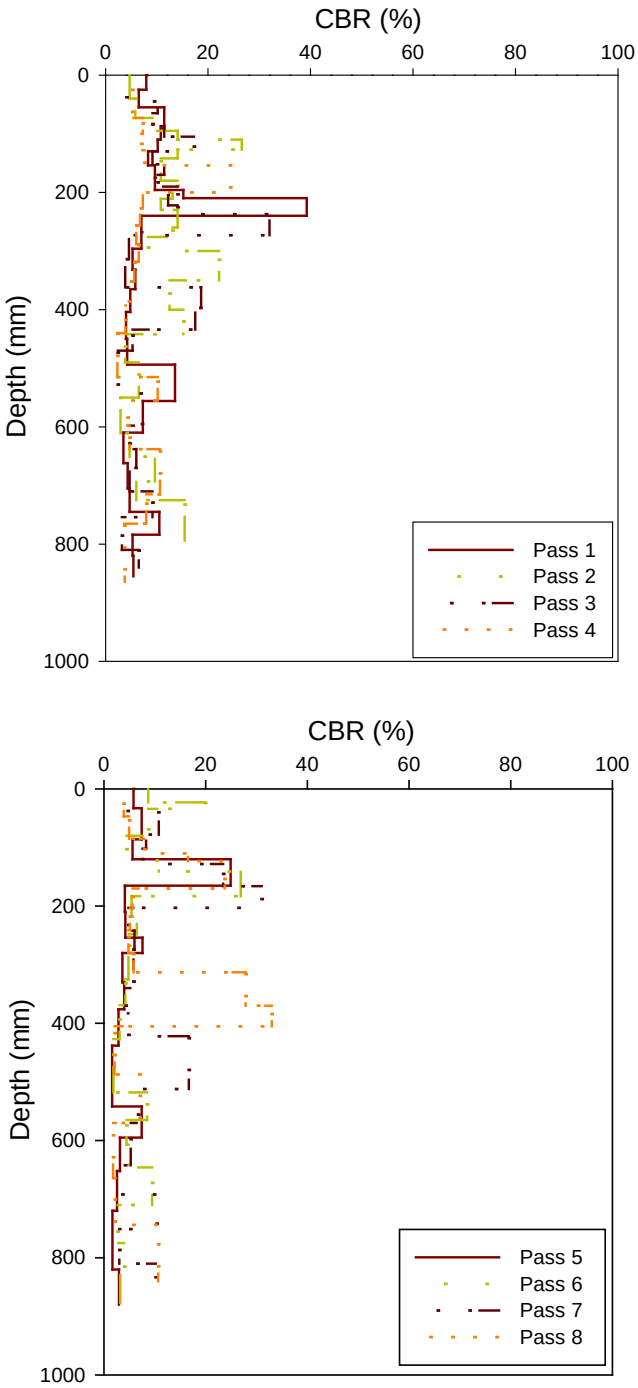

Figure 30. TB2: DCP-CBR profiles after static compaction roller passes

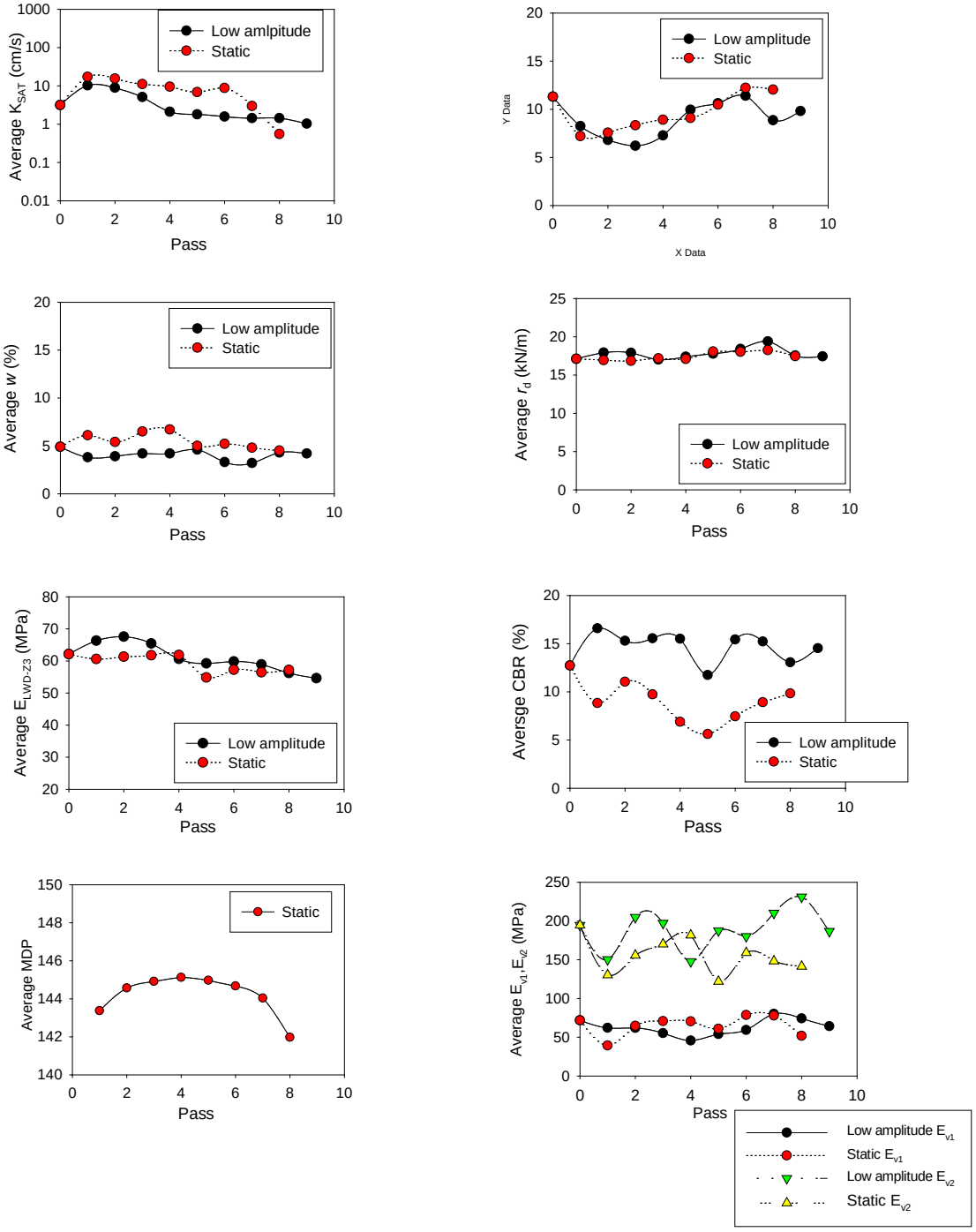

Figure 31. TB2: Comparison of average in situ point measurements after low amplitude vibratory and static compaction roller passes

TB3: Virgin Crushed Limestone and RPCC

MDP* results obtained from TB3 from the two lanes are presented in Figure 32Figure 33. Average MDP* values per pass are shown in Figure 34 for the two lanes. Results indicated that the MDP* values obtained in static mode were higher than in vibratory mode, which was also observed in TB1. As noted earlier, MDP* measurements are influenced by vibration mode.

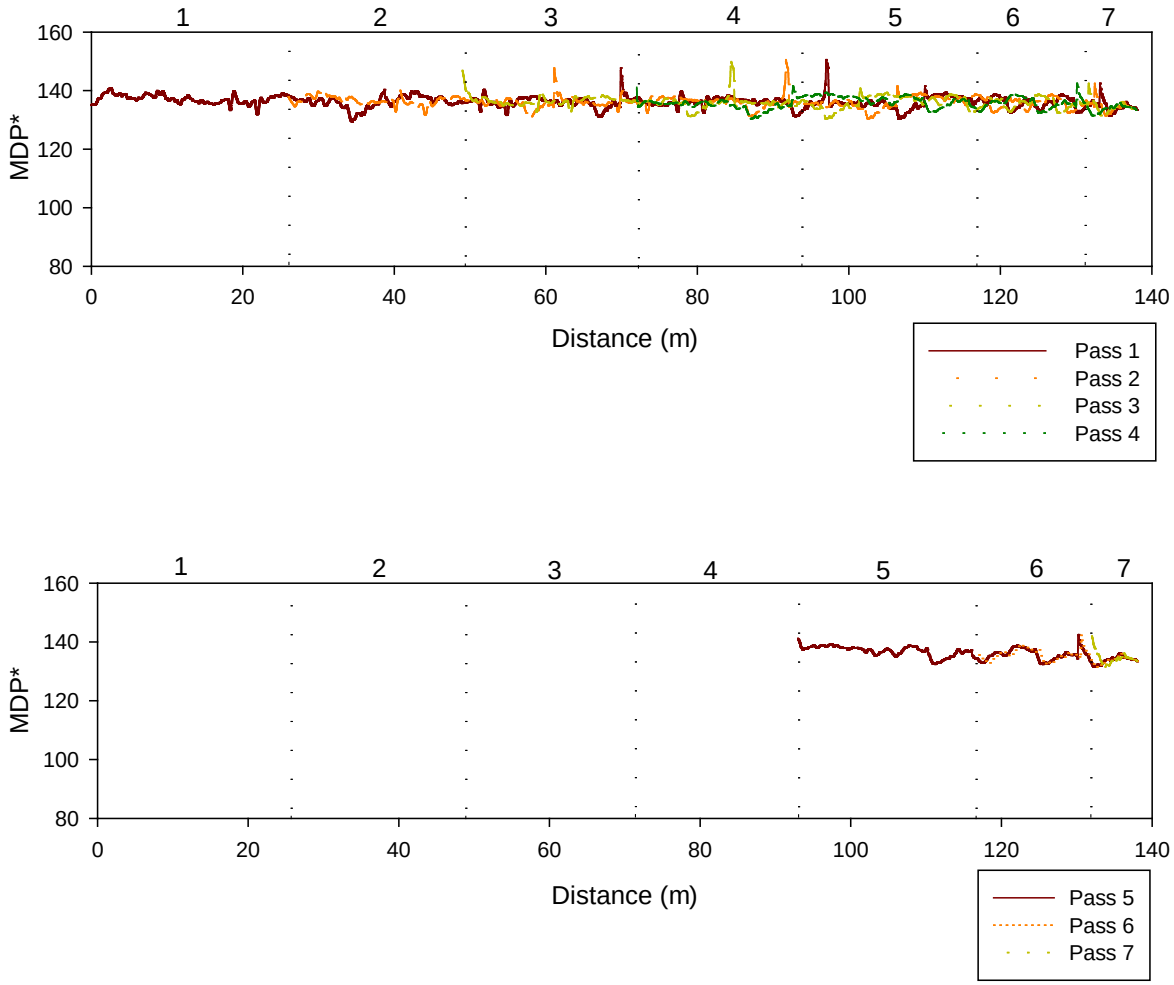

Figure 32. TB3: MDP* compaction curves after low amplitude compaction roller passes

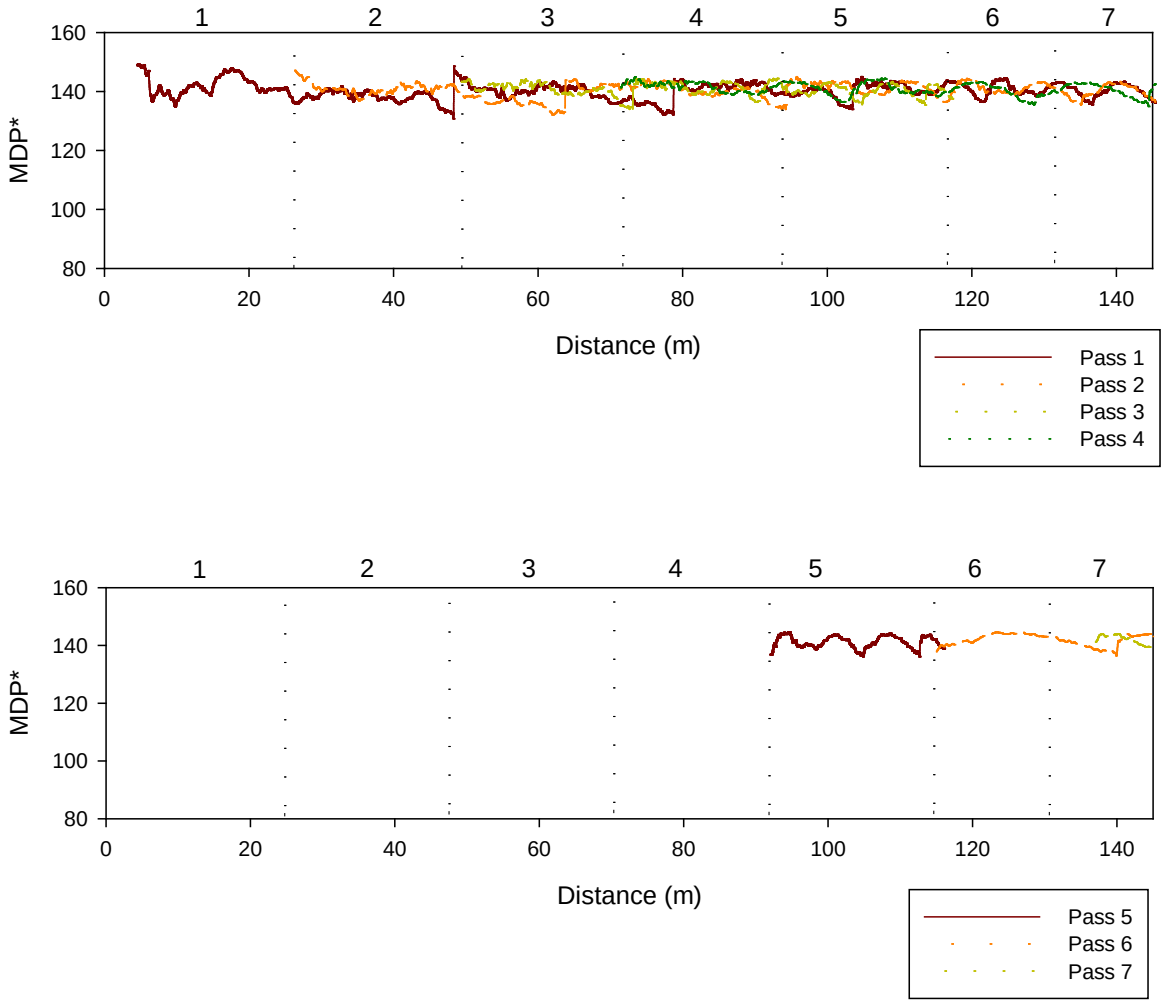

Figure 33. TB3: MDP* compaction curves after static compaction roller passes

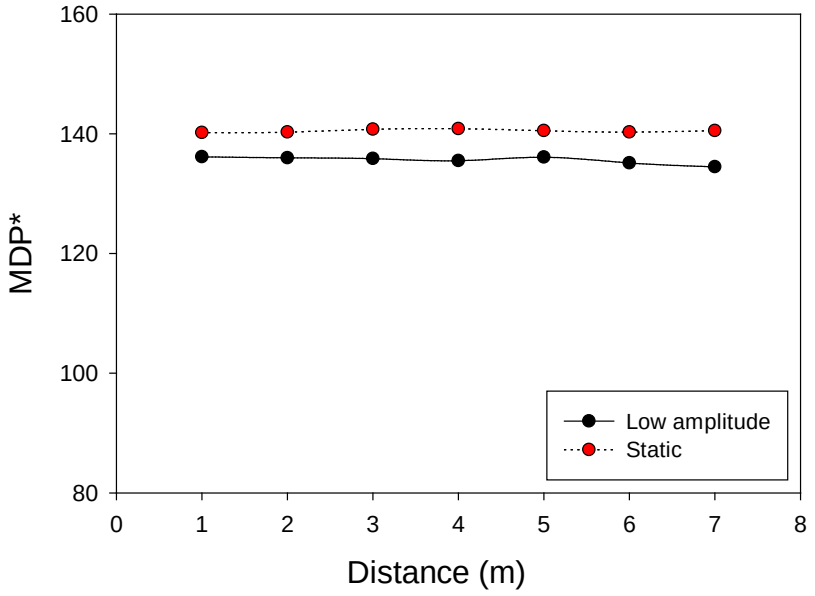

Figure 34. TB3: Comparison of MDP*after low amplitude vibratory and static compaction roller passes

Statistical Analysis Results

In this section, results obtained from TB1 and TB2 are presented as box plots that show the raw data and identify the mean, median, and 5^{th}, 25^{th}, 75^{th}, and 95^{th} percentiles. Box plots are presented for each measurement value separately in Figure 35 to Figure 42.

The results are analyzed using t-tests to assess if statistically significant differences exist between the different test lanes. Comparisons are made between untrimmed (UT) and trimmed (TM) base layers, and low amplitude (LA) versus static (ST) compaction lanes. Results of statistical t-test analysis are shown in Table 3 and Table 4 for these two comparison cases. These tables also summarize the mean and coefficient of variation (COV) of the measurement values.

Following are the key findings from the statistical analysis:

- On UT base, CBR, γ_d, F_{200}, $E_{LWD\text{-}Z3}$, and E_{V1} showed statistically significant differences in the measurement values between low amplitude and static mode of compaction. The lane compacted with low amplitude mode resulted in higher values. There was no statistically significant difference in the *k*, K_{sat}, E_{v2}, and *w* measurements.

- On TM base, only K_{sat}, E_{v2}, and *w* measurements showed statistically significant differences between low amplitude and static compaction lanes. The lane compacted in static mode showed higher K_{sat} values. E_{v2} was higher in low amplitude compaction lane.

There was no statistically significant difference between the static and low amplitude compaction lanes in the remaining measurements.

- For lanes compacted using low amplitude vibration, all measurements except CBR showed statistically significant differences between UT and TM base. γ_d, F_{200}, $E_{LWD\text{-}Z3}$, k, Ev_1 and E_{v2} were higher in TM base, while K_{sat} was lower in TM base. These results indicate that trimming process resulted in higher fines content, and a denser and stiffer base layer but decreased the permeability values.

- For lanes compacted in static mode, the t-test results show similar conclusions as the above case with low amplitude compaction. All measurements except CBR showed statistically significant differences between UT and TM base. γ_d, F_{200}, $E_{LWD\text{-}Z3}$, k, Ev_1 and E_{v2} were higher in TM base, while K_{sat} was lower in TM base.

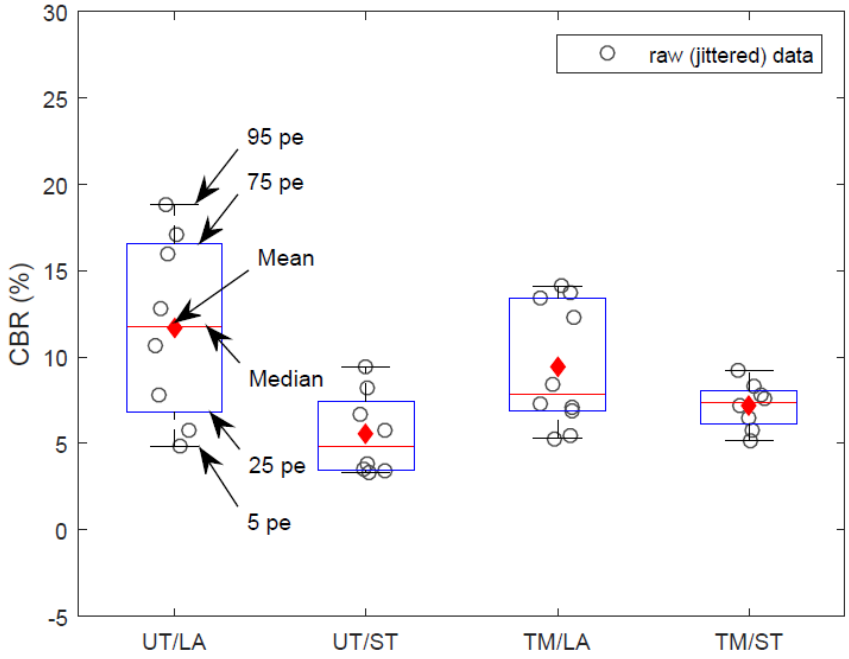

Figure 35. Box plots of DCP-CBR (UT indicates untrimmed; LA indicates low amplitude; TM indicates trimmed; ST indicates static)

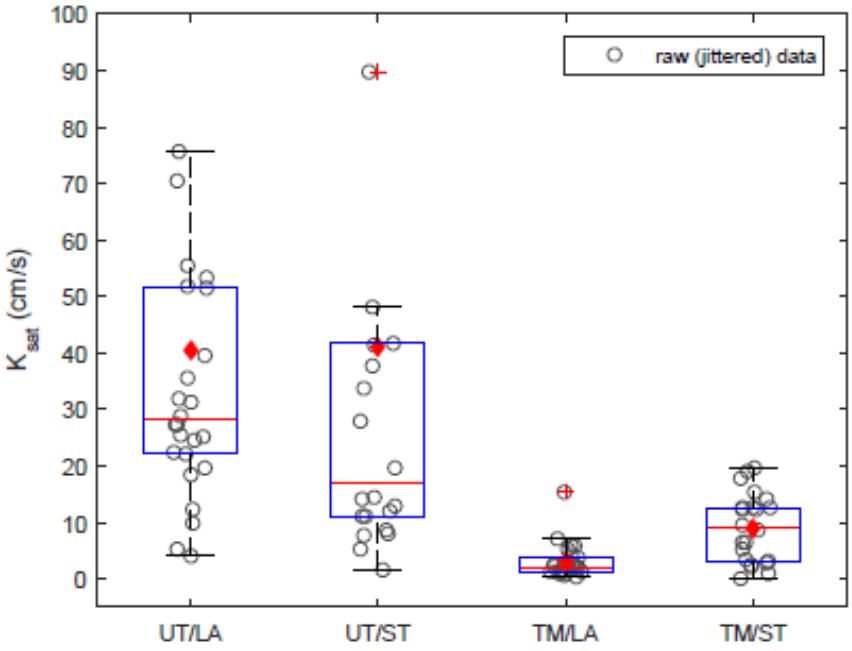

Figure 36. Box plots of K_{sat} (UT indicates untrimmed; LA indicates low amplitude; TM indicates trimmed; ST indicates static)

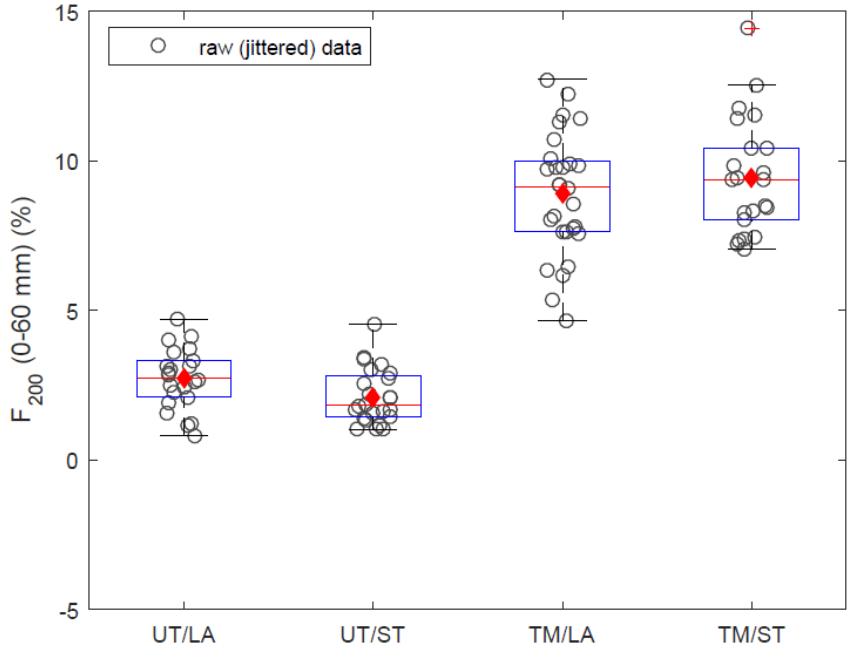

Figure 37. Box plots of fines content, F_{200} (0-60 mm) (UT indicates untrimmed; LA indicates low amplitude; TM indicates trimmed; ST indicates static)

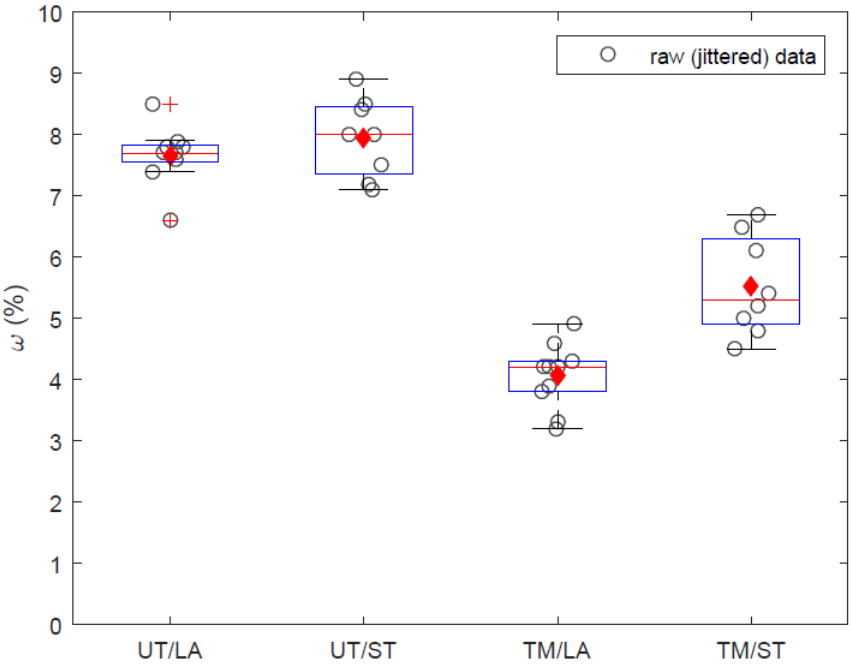

Figure 38. Box plots of moisture content, *w* (UT indicates untrimmed; LA indicates low amplitude; TM indicates trimmed; ST indicates static)

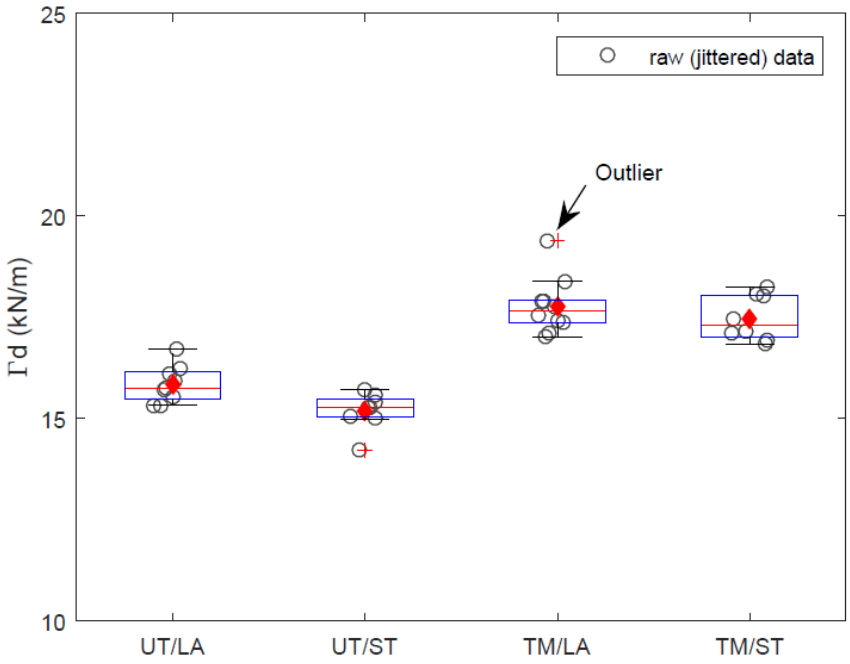

Figure 39. Box plots of density, γ_d (UT indicates untrimmed; LA indicates low amplitude; TM indicates trimmed; ST indicates static)

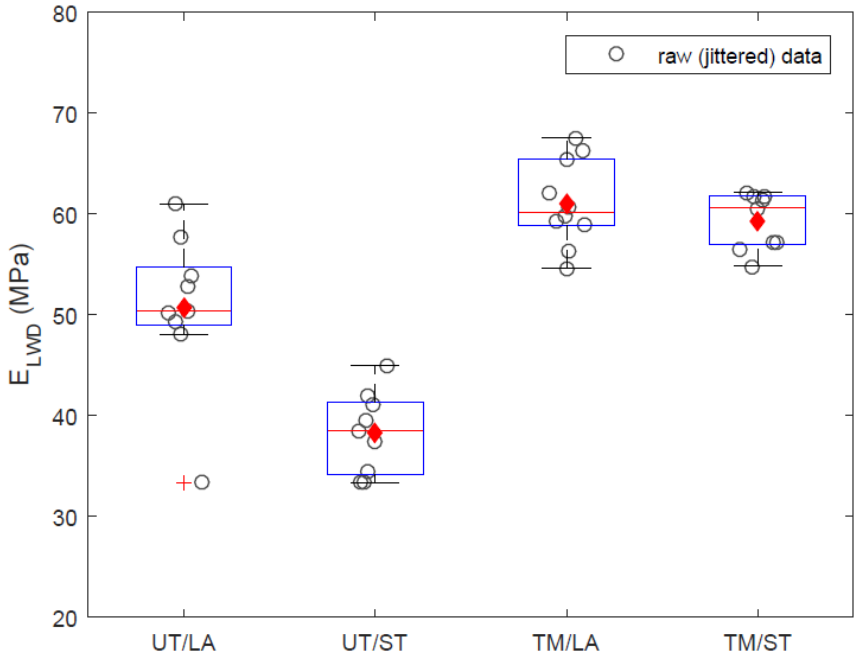

Figure 40. Box plots of $E_{LWD\text{-}Z3}$ (UT indicates untrimmed; LA indicates low amplitude; TM indicates trimmed; ST indicates static)

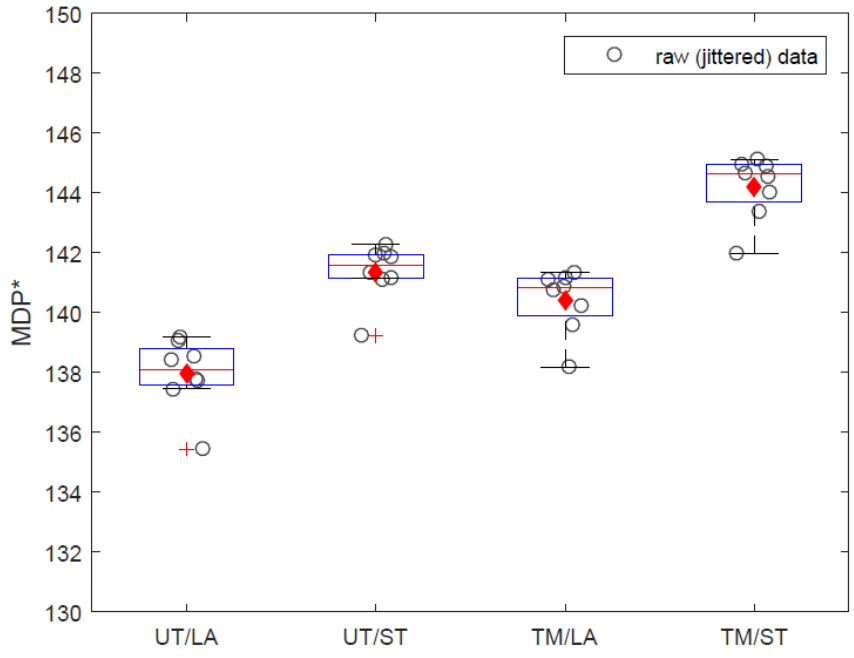

Figure 41. Box plots of MDP* (UT indicates untrimmed; LA indicates low amplitude; TM indicates trimmed; ST indicates static)

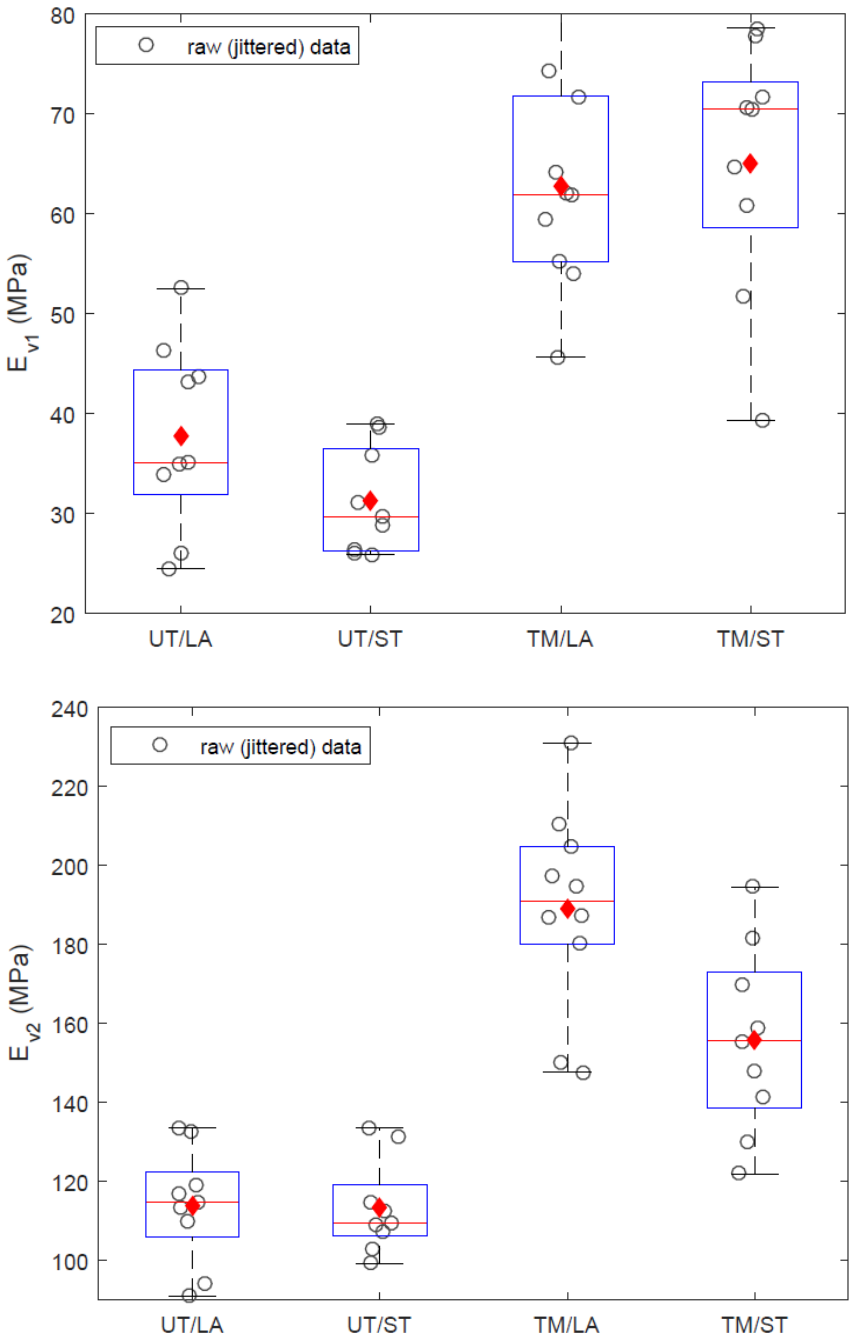

Figure 42. Box plots of E_{v1} and E_{v2} (UT indicates untrimmed; LA indicates low amplitude; TM indicates trimmed; ST indicates static)

Table 3. Summary of t-test results to compare low amplitude (LA) and static (ST) compaction on untrimmed base (UT)

Parameter	Condition	Mean	COV (%)	t	P_r	Condition	Mean	COV (%)	t	P_r
CBR (%)	UT/LA	11.7	45	3.01	0.007	TM/LA	9.4	38	1.80	0.048
	UT/ST	5.5	43			TM/ST	7.2	18		
γ_d (kN/m^3)	UT/LA	15.85	3	2.97	0.005	TM/LA	17.78	4	1.05	0.16
	UT/ST	15.18	3			TM/ST	17.47	3		
F_{200} (%)	UT/LA	2.7	37	2.13	0.019	TM/LA	8.9	23	-1.02	0.16
	UT/ST	2.1	44			TM/ST	9.5	21		
k-value (kPa/mm)	UT/LA	54.6	25	1.62	0.064	TM/LA	90.8	16	-0.24	0.406
	UT/ST	46.1	16			TM/ST	92.8	21		
K_{sat} (cm/s)	UT/LA	40.4	87	-0.05	0.482	TM/LA	3.1	103	-4.14	< 0.001
	UT/ST	41.0	124			TM/ST	9.0	67		
E_{LWD-Z3} (MPa)	UT/LA	50.7	15	4.26	0.001	TM/LA	61.1	7	1.11	0.141
	UT/ST	38.3	11			TM/ST	59.2	5		
MDP*	UT/LA	138.0	1	-6.33	< 0.001	TM/LA	140.4	1	-7.11	< 0.001
	UT/ST	141.4	1			TM/ST	144.2	1		
E_{v1} (MPa)	UT/LA	38.0	25	1.83	0.046	TM/LA	63	16	-0.42	0.34
	UT/ST	31.0	17			TM/ST	65	20		
E_{v2} (MPa)	UT/LA	113.9	13	0.09	0.467	TM/LA	189.0	14	2.95	0.004
	UT/ST	113.4	10			TM/ST	155.8	15		
w (%)	UT/LA	7.7	7	-1.01	0.167	TM/LA	4.1	13	-4.40	< 0.001
	UT/ST	8.0	8			TM/ST	5.5	15		

Notes: UT indicates untrimmed; LA indicates low amplitude; TM indicates trimmed; ST indicates static. Cells highlighted indicate statistical significance at the 95% confidence level.

Table 4. Summary of t-test results to compare low amplitude compaction (LA) on untrimmed (UT) base and trimmed (TM) base

Parameter	Condition	Mean	COV (%)	t	P_r	Condition	Mean	COV (%)	t	P_r
CBR (%)	UT/LA	11.7	45	1.06	0.155	UT/ST	5.5	43	-1.75	0.054
	TM/LA	9.4	38			TM/ST	7.2	18		
γ_d (kN/m^3)	UT/LA	15.85	3	-7.21	< 0.001	UT/ST	15.18	3	8.92	< 0.001
	TM/LA	17.78	4			TM/ST	17.47	3		
F_{200} (%)	UT/LA	2.7	37	-13.96	< 0.001	UT/ST	2.1	44	-16.09	< 0.001
	TM/LA	8.9	23			TM/ST	9.5	21		
k-value (kPa/mm)	UT/LA	54.6	25	-5.55	< 0.001	UT/ST	46.1	16	-6.36	< 0.001
	TM/LA	90.8	16			TM/ST	92.8	21		
K_{sat} (cm/s)	UT/LA	40.4	87	5.42	< 0.001	UT/ST	41.0	124	2.93	0.004
	TM/LA	3.1	103			TM/ST	9.0	67		
E_{LWD-Z3} (MPa)	UT/LA	50.7	15	-3.54	0.002	UT/ST	38.3	11	-12.75	< 0.001
	TM/LA	61.1	7			TM/ST	59.2	5		
E_{v1} (MPa)	UT/LA	38	25	-5.55	< 0.001	UT/ST	31	17	-7.34	< 0.001
	TM/LA	63	16			TM/ST	65	20		
E_{v2} (MPa)	UT/LA	113.9	13	-7.96	< 0.001	UT/ST	113.4	10	-4.83	< 0.001
	TM/LA	189.0	14			TM/ST	155.8	15		
w (%)	UT/LA	7.7	7	15.27	< 0.001	UT/ST	8.0	8	6.61	< 0.001
	TM/LA	4.1	13			TM/ST	5.5	15		

Notes: UT indicates untrimmed; LA indicates low amplitude; TM indicates trimmed; ST indicates static. Cells highlighted indicate statistical significance at the 95% confidence level.

CHAPTER 5. SUMMARY AND CONCLUSIONS

The main objective of this field study was to investigate the impacts of vibratory versus static mode of compaction and number of compaction passes on the granular subbase layer material properties such as material fines content, dry density, elastic modulus, California bearing ratio, modulus of subgrade reaction, and saturated hydraulic conductivity. Results from the field testing are presented above and are analyzed using statistical t-test analysis to assess if statistically significant differences exist between untrimmed and trimmed base layers, and low amplitude versus static compaction. Following are the key findings from the field testing analysis:

- On untrimmed granular subbase layer, CBR, γ_d, F_{200}, $E_{LWD\text{-}Z3}$, and E_{V1} showed statistically significant differences in the measurement values between low amplitude and static mode of compaction. The lane compacted with low amplitude mode resulted in higher values. There was no statistically significant difference in the *k*, K_{sat}, E_{v2}, and *w* measurements.
- On trimmed granular subbase layer, only K_{sat}, E_{v2}, and *w* measurements showed statistically significant differences between low amplitude and static compaction lanes. The lane compacted in static mode showed higher K_{sat} values. E_{v2} was higher in low amplitude compaction lane. There were no statistically significant differences in the remaining measurements between the static and low amplitude compaction lanes.
- For lanes compacted using low amplitude vibration, all measurements except CBR showed statistically significant differences between UT and TM base. γ_d, F_{200}, $E_{LWD\text{-}Z3}$, *k*, Ev_1 and E_{v2} were higher in TM base, while K_{sat} was lower in TM base.
- For lanes compacted in static mode, the t-test results show similar conclusions as the above case with low amplitude compaction. All measurements except CBR showed statistically significant differences between UT and TM base. γ_d, F_{200}, $E_{LWD\text{-}Z3}$, *k*, Ev_1 and E_{v2} were higher in TM base, while K_{sat} was lower in TM base.

These results indicate that the use of low amplitude vibration instead of the static mode of compaction can result in material degradation, as evidenced by increases in fines contents, but the resulting fines content were within the specified gradation limits. However, the trimming process resulted in much higher fines content, which in turn resulted in a denser and stiffer subbase layer but also decreased permeability values

REFERENCES

AASHTO. (1993). *AASHTO design guide for design of pavement structures*. American Association of State Highway and Transportation Officials, Washington DC.

ASTM C136-06. (2010). "Standard test method for sieve analysis of fine and coarse aggregates." American Standards for Testing Methods (ASTM), West Conshohocken, PA.

ASTM D6951-03 (2010). "Standard test method for use of the dynamic cone penetrometer in shallow pavement applications." American Standards for Testing Methods (ASTM), West Conshohocken, PA.

ASTM D6938-10. (2010). "Standard test method for in-place density and water content of soil and soil-aggregate by nuclear methods (shallow depth)." American Standards for Testing Methods (ASTM), West Conshohocken, PA.

Iowa DOT. (2016a). Section 4121. Granular Subbase Material. *Standard Specifications with GS-15002 revisions*. <http://www.iowadot.gov/erl/archives/apr_2007/GS/content/4121.htm> (Accessed May 2016).

Iowa DOT. (2016b). Section 2111. Granular Subbase. *Standard specifications with GS-15002 Revisions.* <http://www.iowadot.gov/erl/archives/apr_2006/GS/content/2111.htm> (Accessed May 2016).

Ott, R., and M. Longnecker. (2008). *An introduction to statistical methods and data analysis*. Cengage Learning.

PCA. (1984). *Thickness design for concrete highway and street pavements,* Portland Cement Association, Skokie, IL.

Terzaghi, K., and R. B. Peck. (1967). *Soil mechanics in engineering practice*, 2nd Ed., John Wiley & Sons, Inc., New York.

Thompson, M., and D. White. (2008). "Estimating compaction of cohesive soils from machine drive power." *Journal of Geotechnical and Geoenvironmental Engineering*, ASCE, 134(12), 1771–1777.

Vennapusa, P., and D. J. White. (2009). "Comparison of light weight deflectometer measurements for pavement foundation materials." *Geotechnical Testing Journal*, ASTM, 32(3), 239–251.

Vennapusa, P., D. J. White, and H. Gieselman. (2009). Influence of support conditions on roller-integrated machine drive power measurements for granular base. International Foundation Congress and Equipment Exposition 2009 (IFCEE 09). March 15-19, Orlando, FL.

White, D. J., and M. Thompson. (2008). "Relationships between in situ and roller-integrated compaction measurements for granular soils." *Journal of Geotechnical and Geoenvironmental Engineering*, ASCE, 134(2), 1763–1770.

White, D. J., E. Jaselskis, V. Schaefer, T. Cackler, (2005). "Real-time compaction monitoring in cohesive soils from machine response." *Transportation Research Record: Journal of the Transportation Research Board.* No. 1936, Transportation Research Board of the National Academies, Washington DC, 173-180.

White, D. J., P. Vennapusa, M. T. Suleiman., and C. T. Jahren. (2007). "An in situ device for rapid determination of permeability for granular bases." *Geotechnical Testing Journal*, 30(4), 282–291.

White, D. J., P. Vennapusa, D. Eichner, H. Gieselman, L. Zhao, and C. T. Jahren. (2010a). *Rapid, self-contained in situ permeameter for field QA/QC of pavement base/subbase materials.* NCHRP 1-130 IDEA Project, Transportation Research Board, Washington, DC.

White, D. J., P. Vennapusa, H. Gieselman, J. Zhang, R. Goldsmith, L. Johanson, and S. Quist. (2010b). *Accelerated Implementation of Intelligent Compaction Monitoring Technology for Embankment Subgrade Soils, Aggregate Base, and Asphalt Pavement Materials.* TPF-5(128) – *New York IC Demonstration Field Project*, ER10-01, Report submitted to The Transtec Group, FHWA, January.

Witczak, M. W., and J. Uzan. (1988). *The universal airport design system – Report I of IV: Granular material characterization*. Department of Civil Engineering, University of Maryland, College Park. MD.

Zapata and W. N. Houston. (2008). *Calibration and Validation of the Enhanced Integrated Climatic Model for Pavement Design.* NCHRP Report 602, Transportation Research Board, Washington, DC.

Zorn, G. (2003). *Operating manual: Light drop-weight tester ZFG2000*, Zorn Stendal, Germany.

APPENDIX: STRESS-STRAIN CURVES FROM PLATE LOAD TESTS

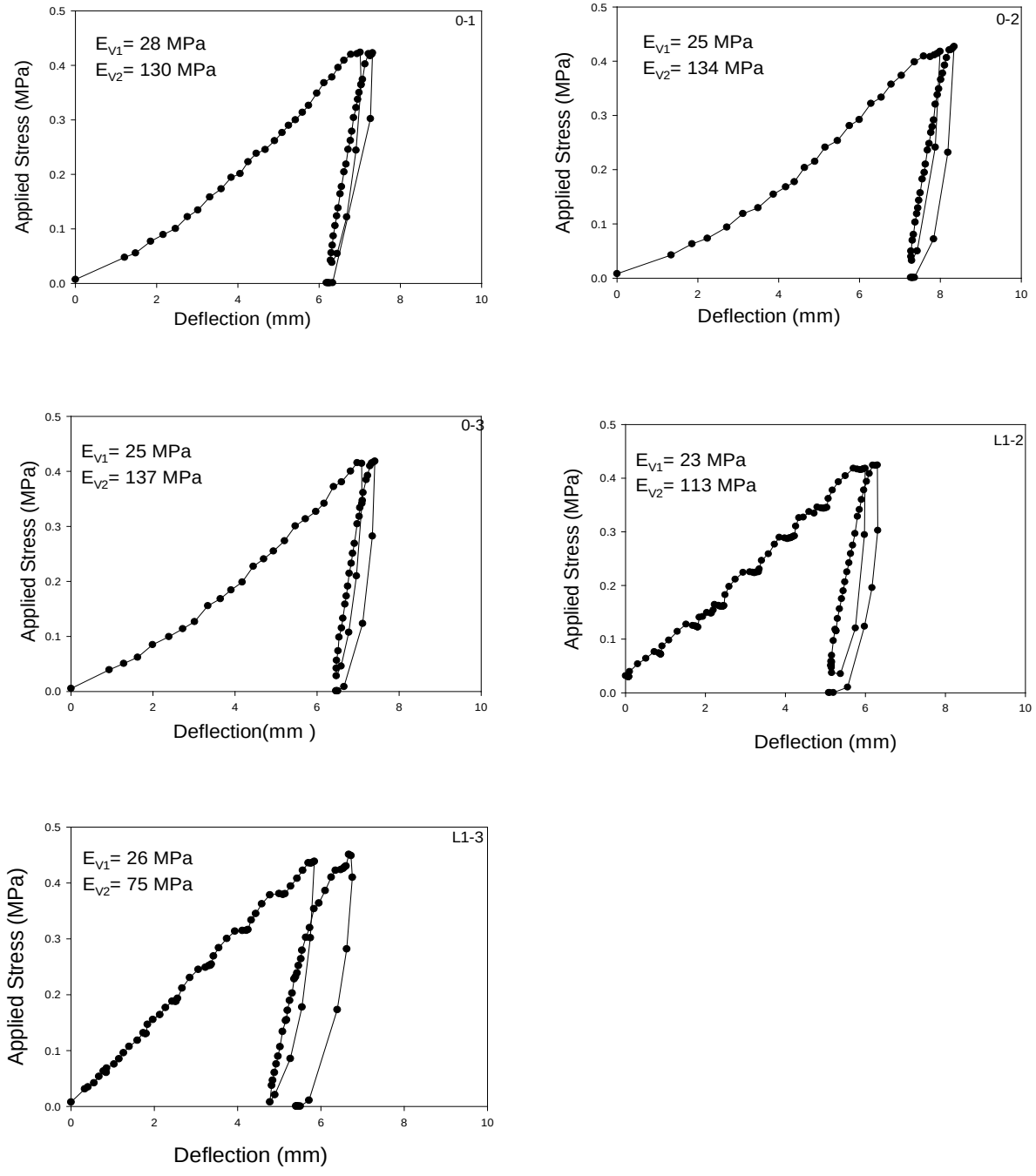

Figure 43. TB1: Stress-strain curves after low amplitude vibratory compaction (0, 1)

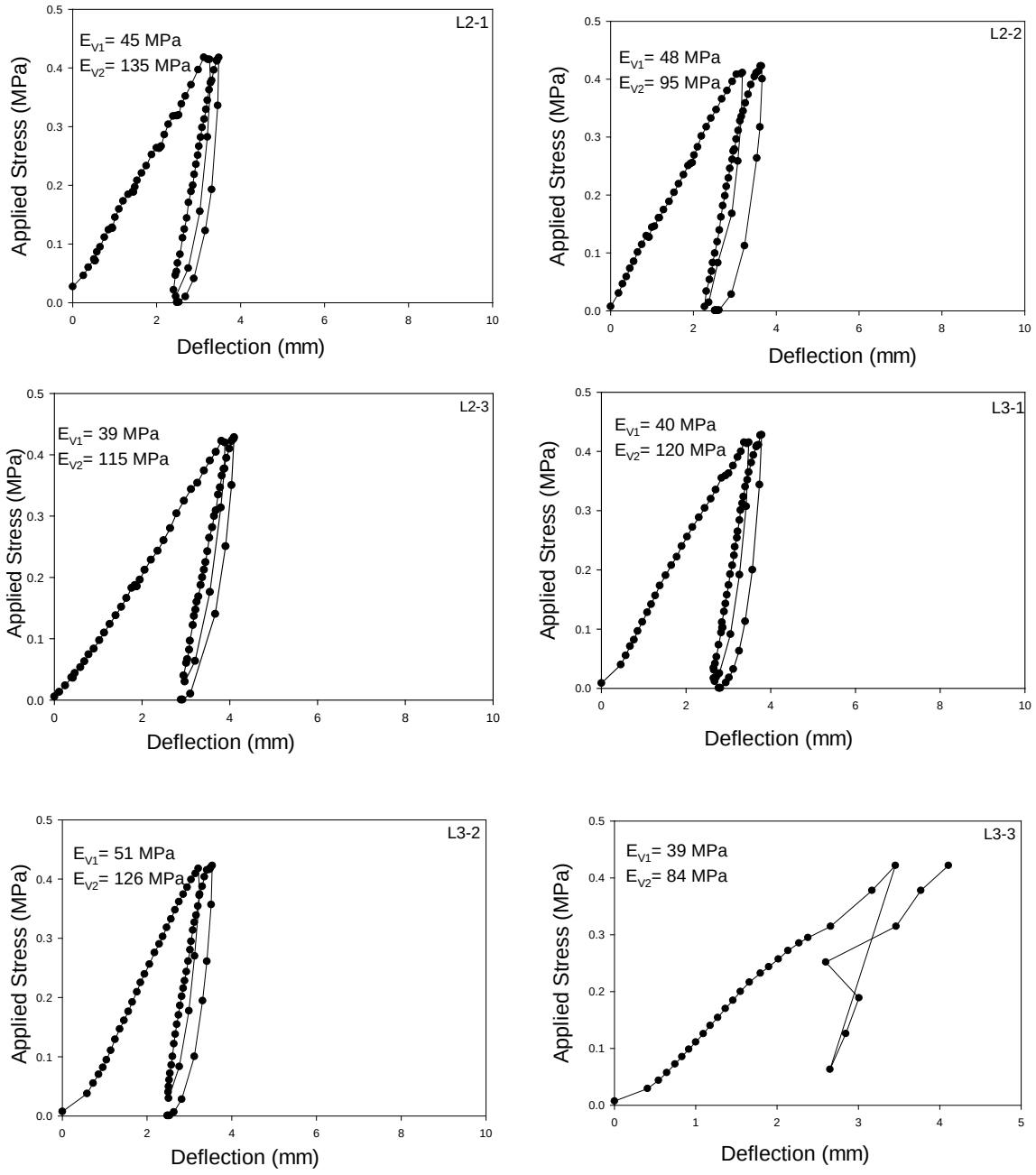

Figure 44. TB1: Stress-strain curves after low amplitude vibratory compaction (2, 3)

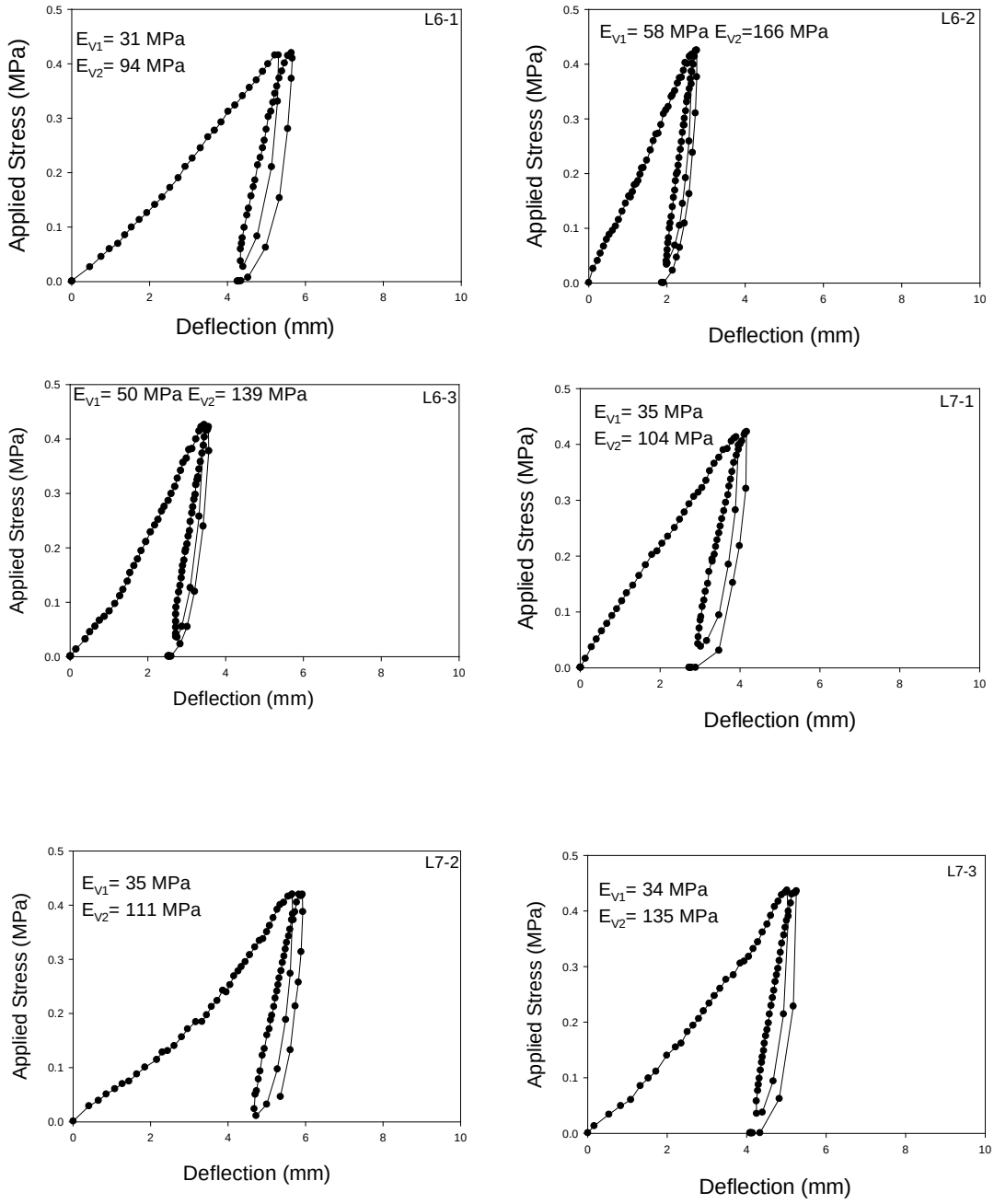

Figure 45. TB1: Stress-strain curves after low amplitude vibratory compaction (6, 7)

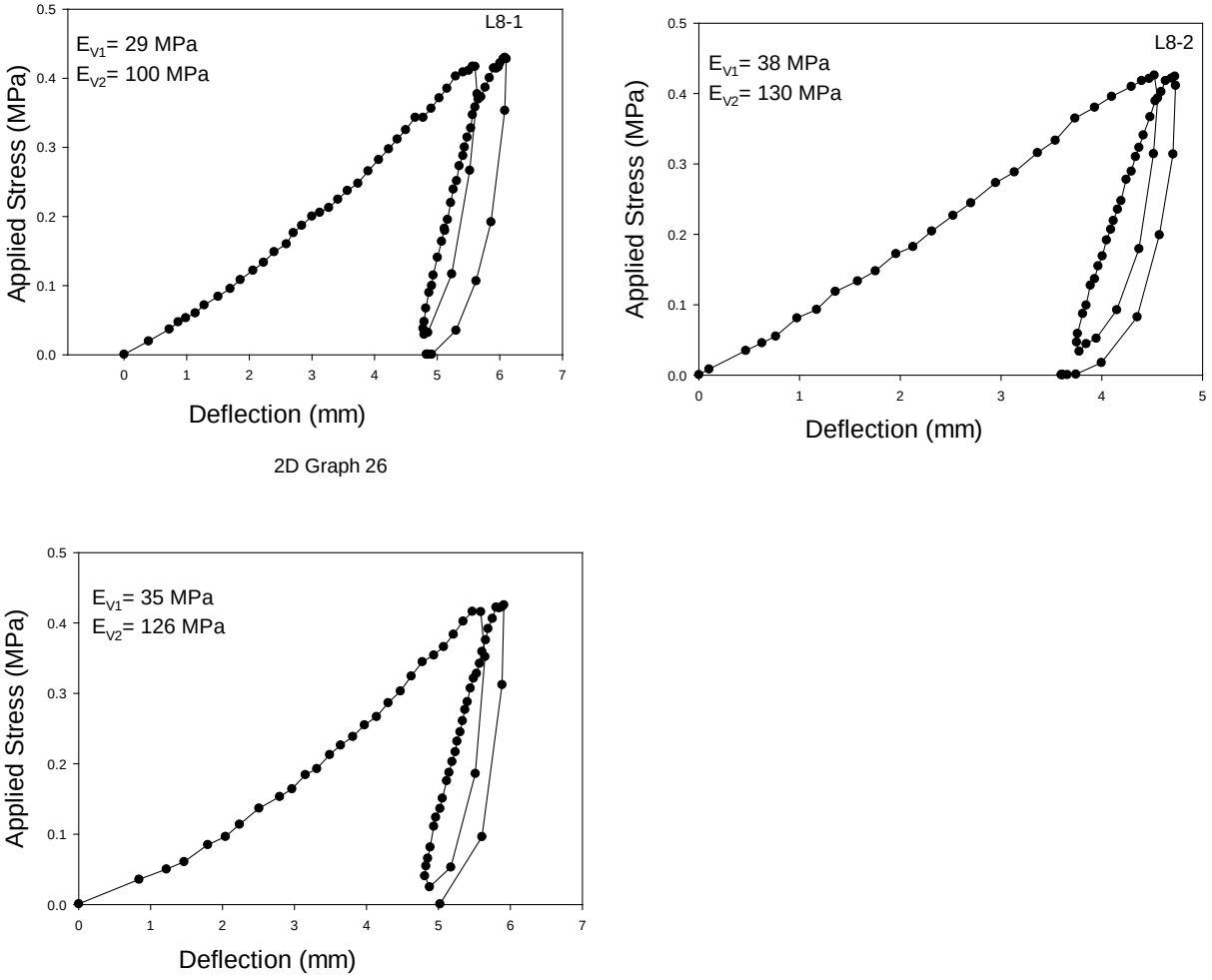

Figure 46. TB1: Stress-strain curve after low amplitude vibratory compaction (8, 9)

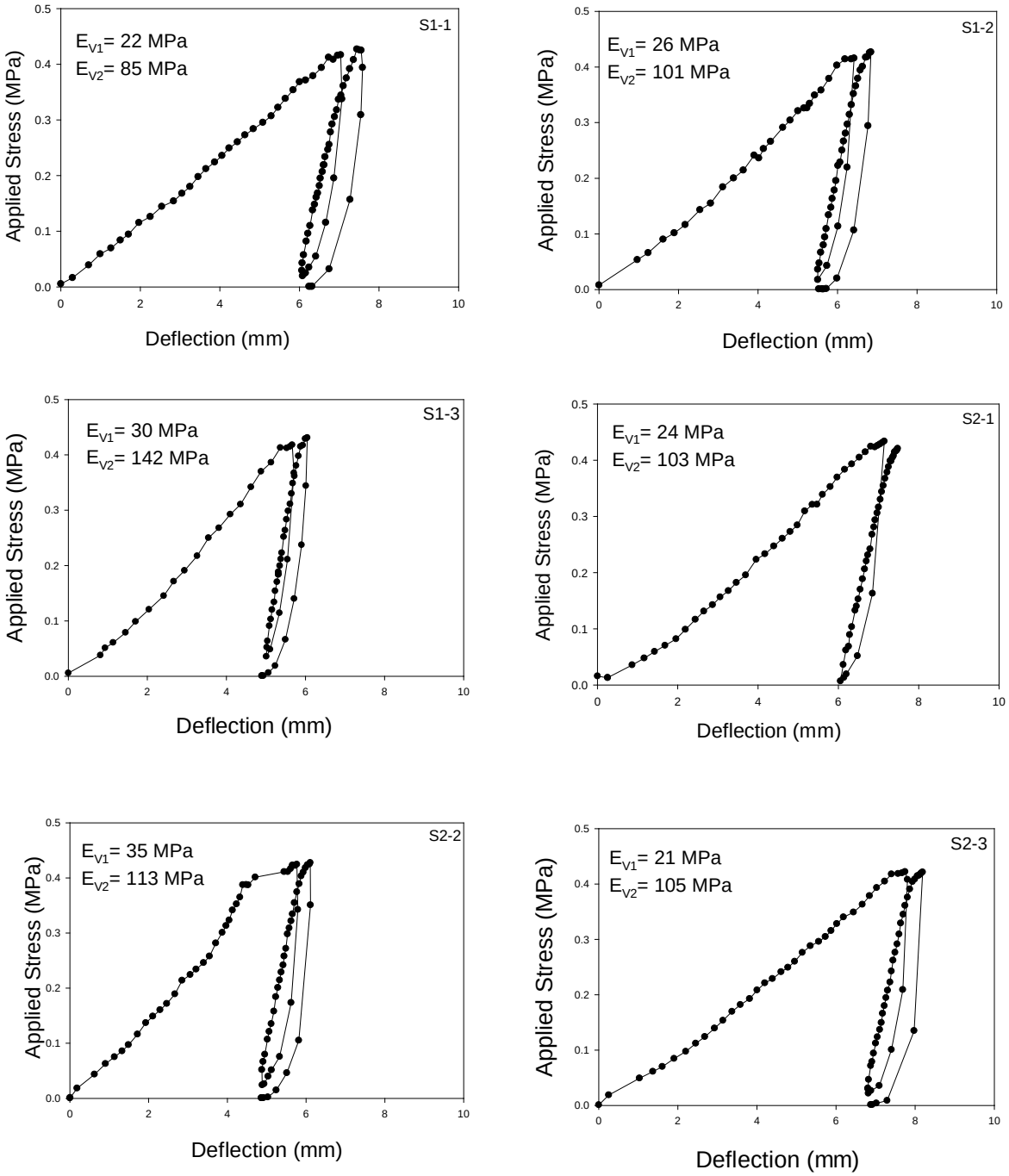

Figure 47. TB1: Stress-strain curves after static compaction (1, 2)

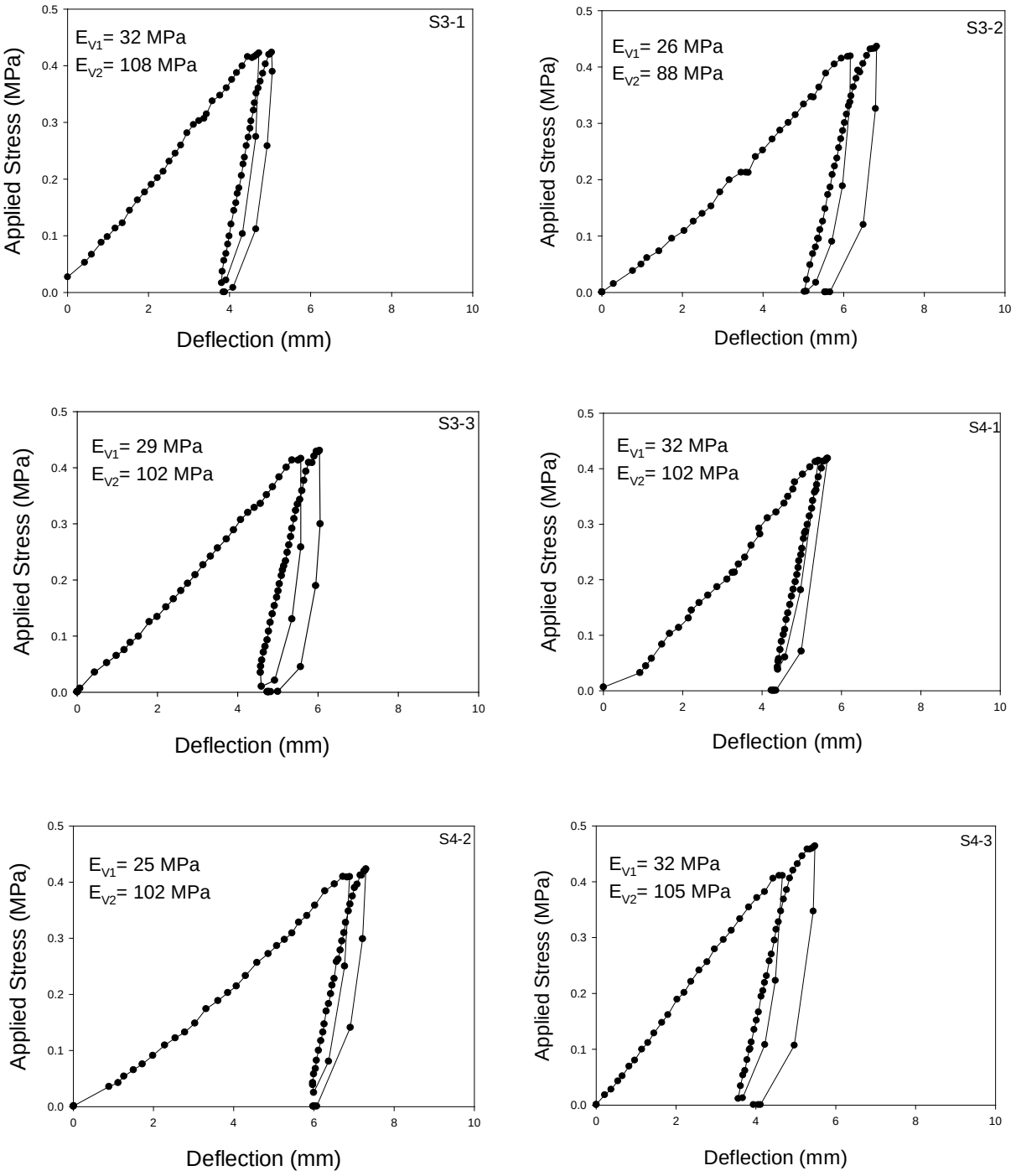

Figure 48. TB1: Stress-strain curves after static compaction (3, 4)

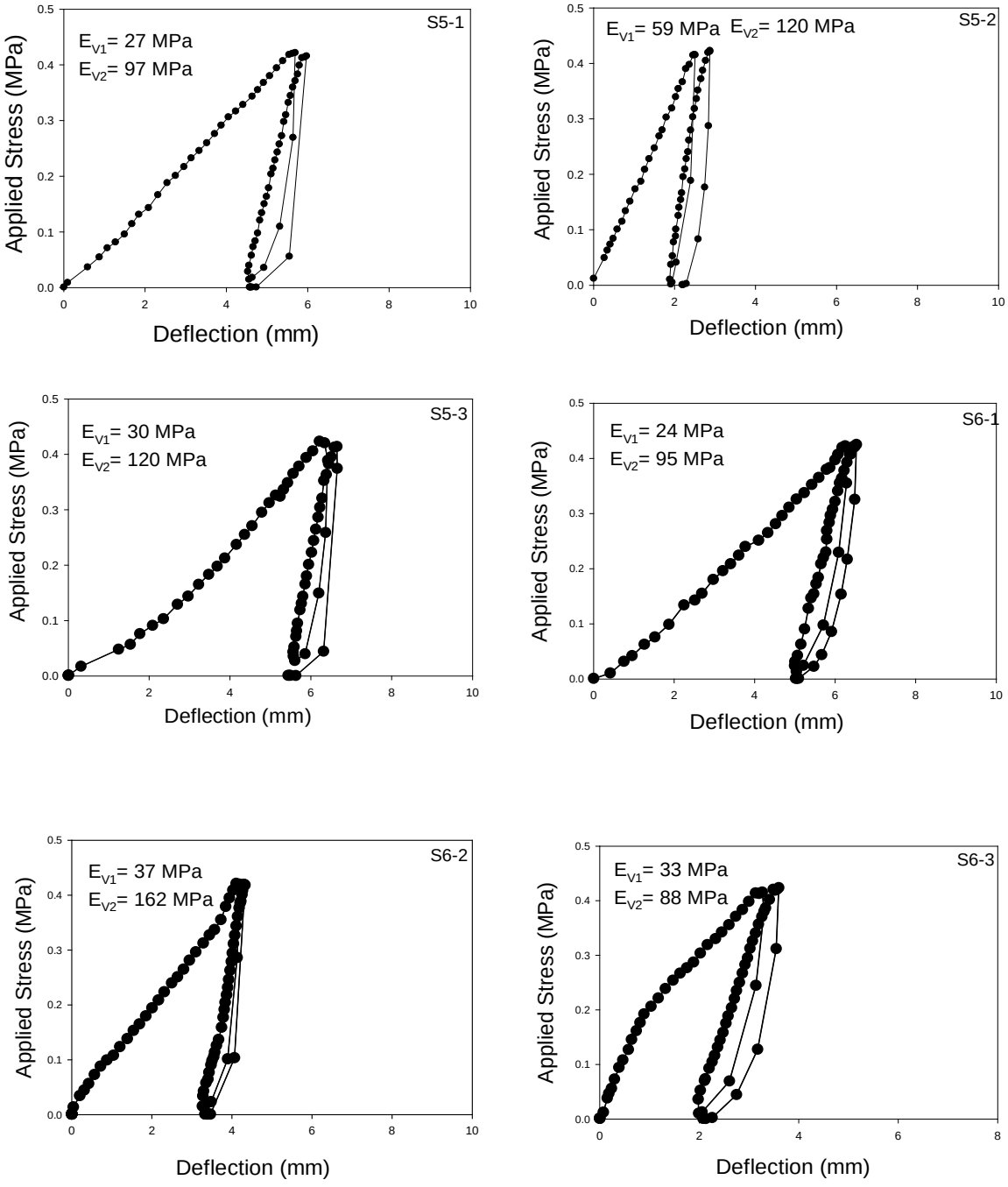

Figure 49. TB1: Stress-strain curves after static compaction (5, 6)

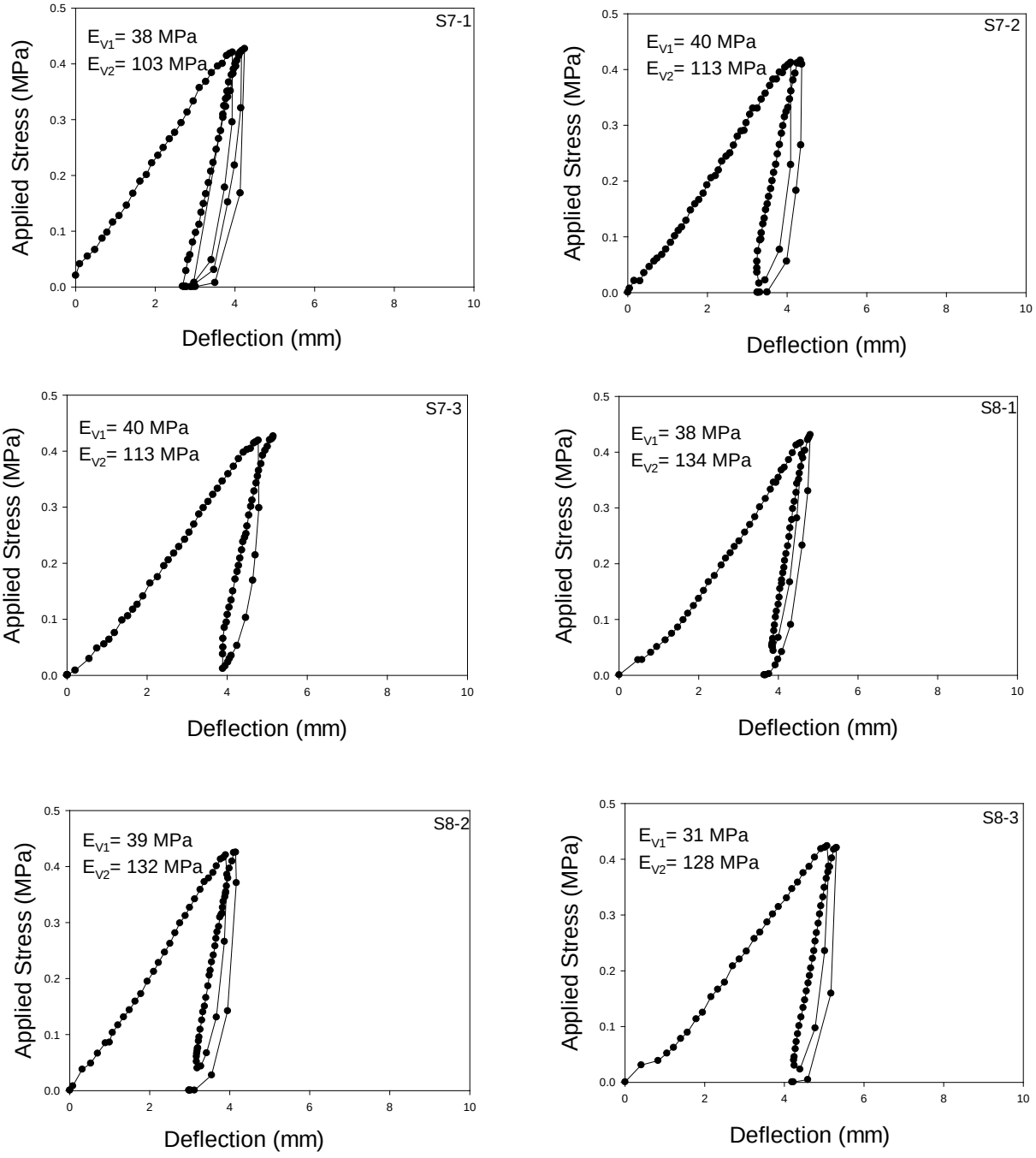

Figure 50. TB1: Stress-strain curves after static compaction (7, 8)

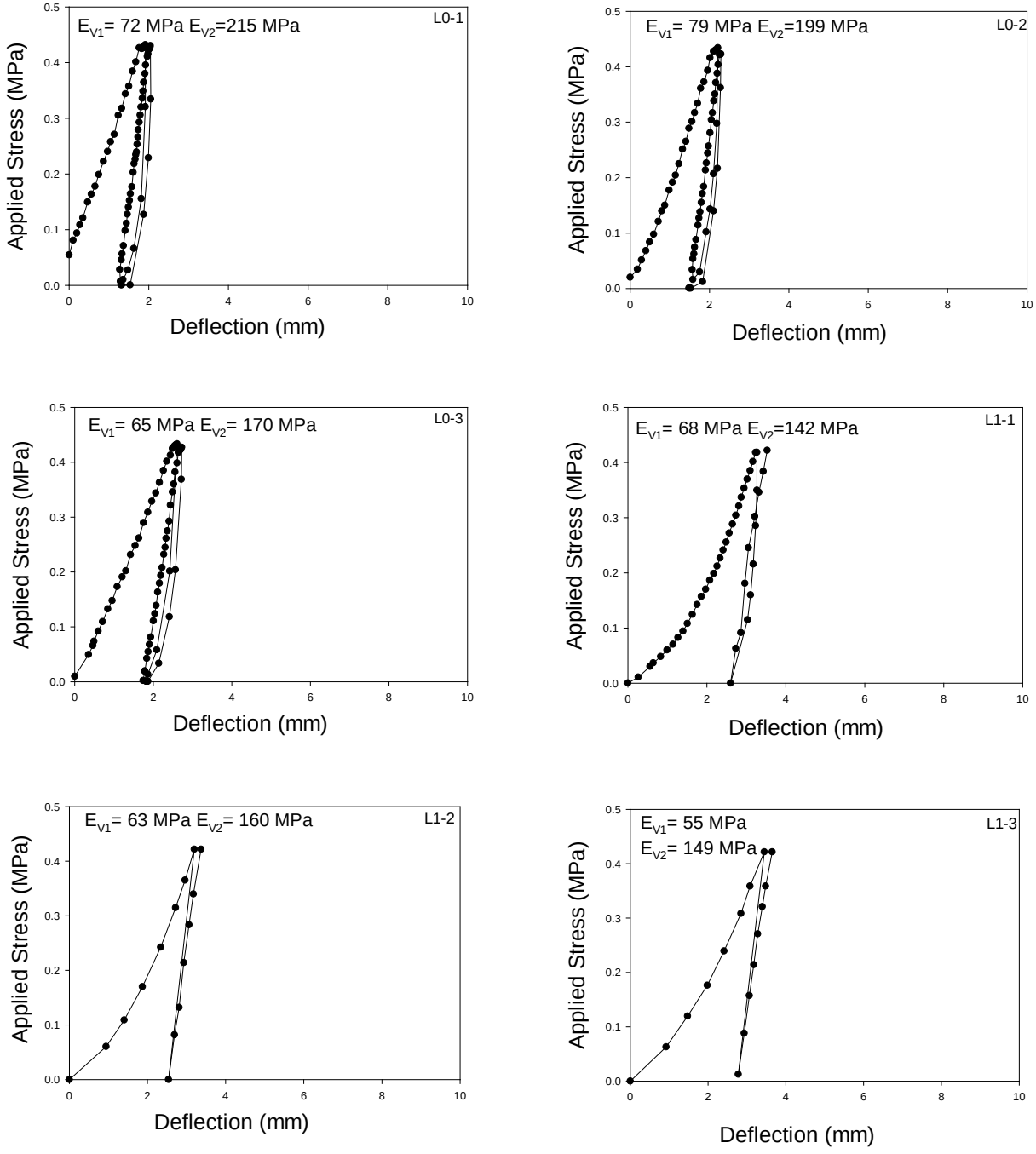

Figure 51. TB2: Stress-strain curves after low amplitude vibratory compaction (0, 1)

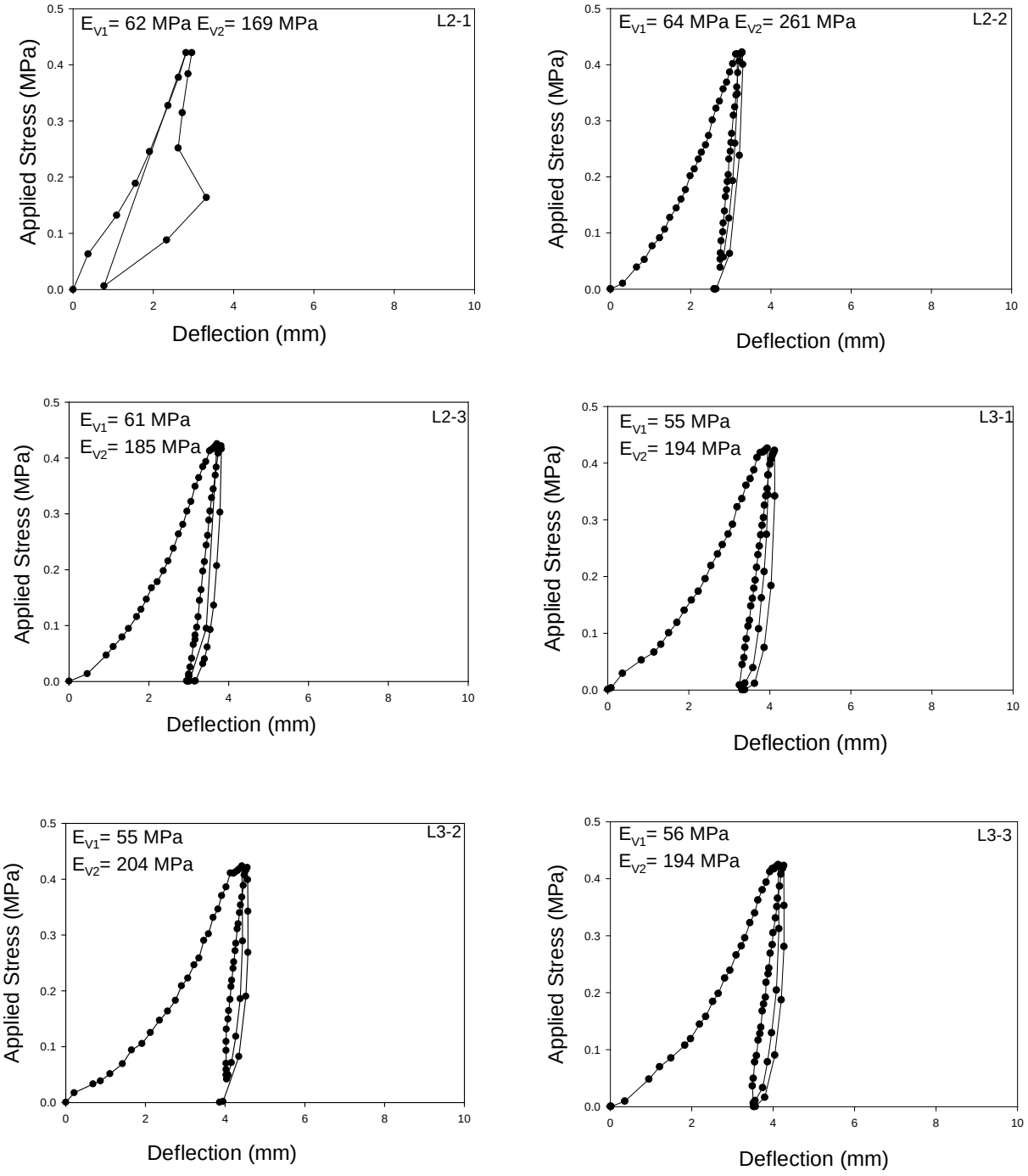

Figure 52. TB2: Stress-strain curves after low amplitude vibratory compaction (2, 3)

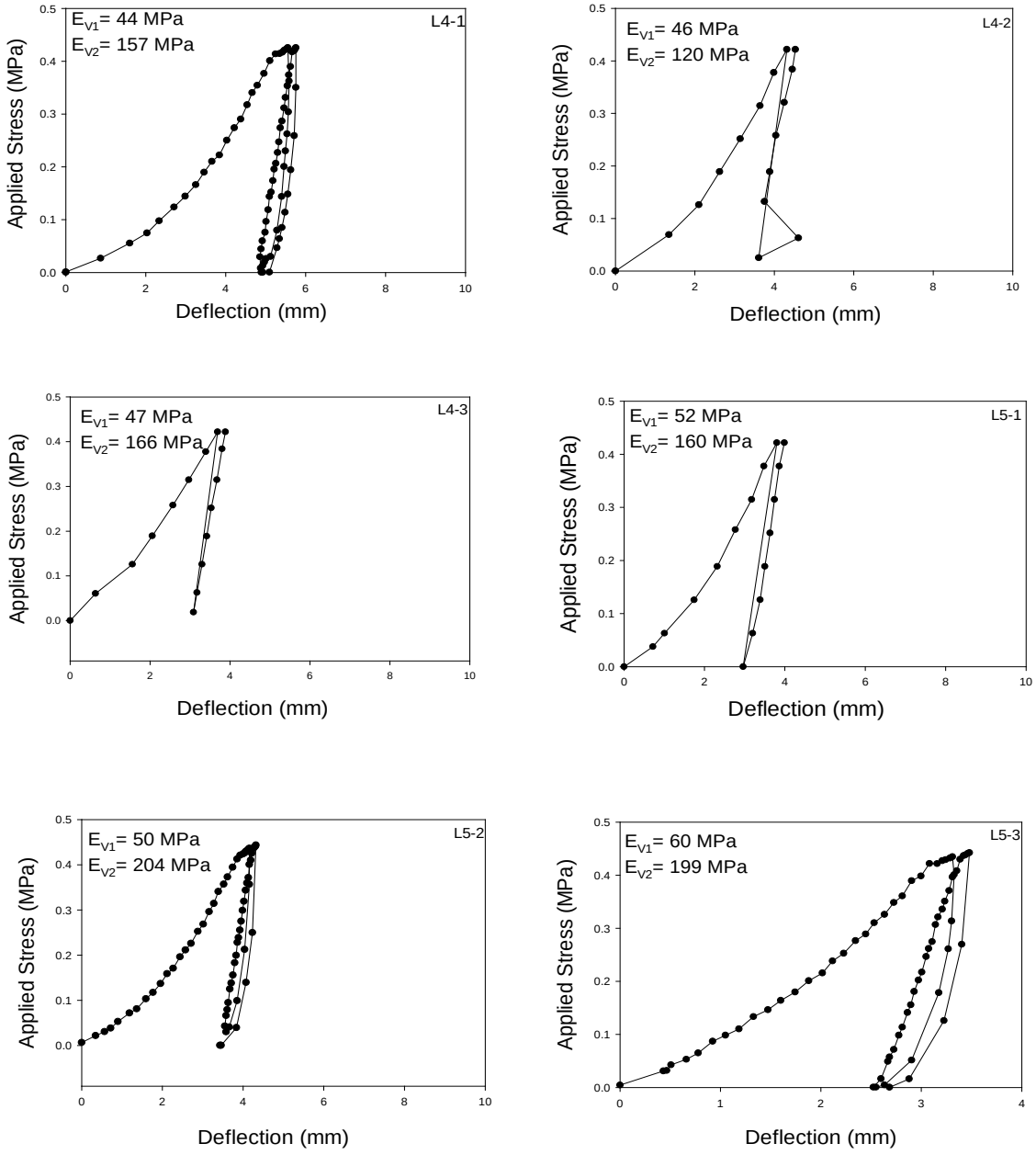

Figure 53. TB2: Stress-strain curves after low amplitude vibratory compaction (4, 5)

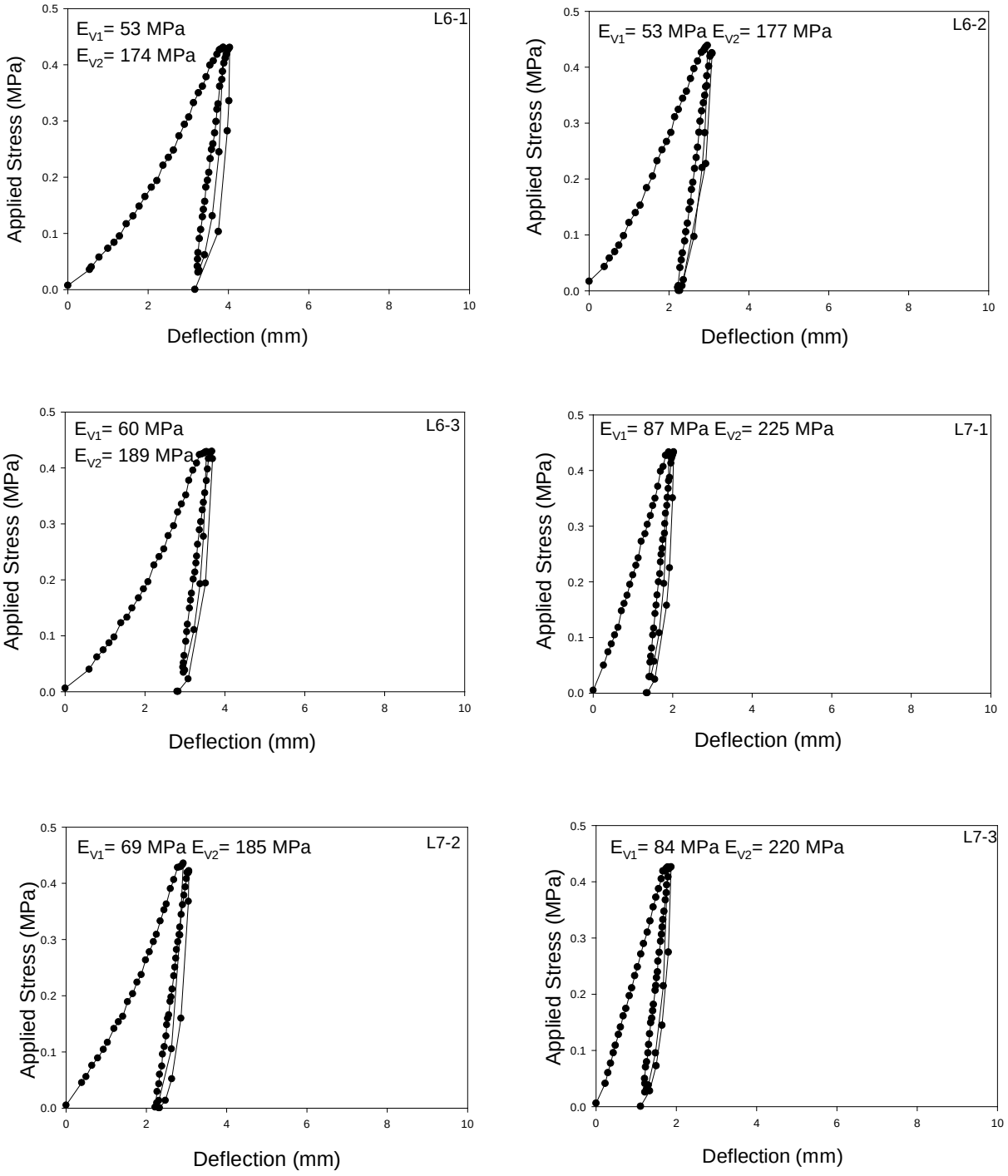

Figure 54. TB2: Stress-strain curves after low amplitude vibratory compaction (6, 7)

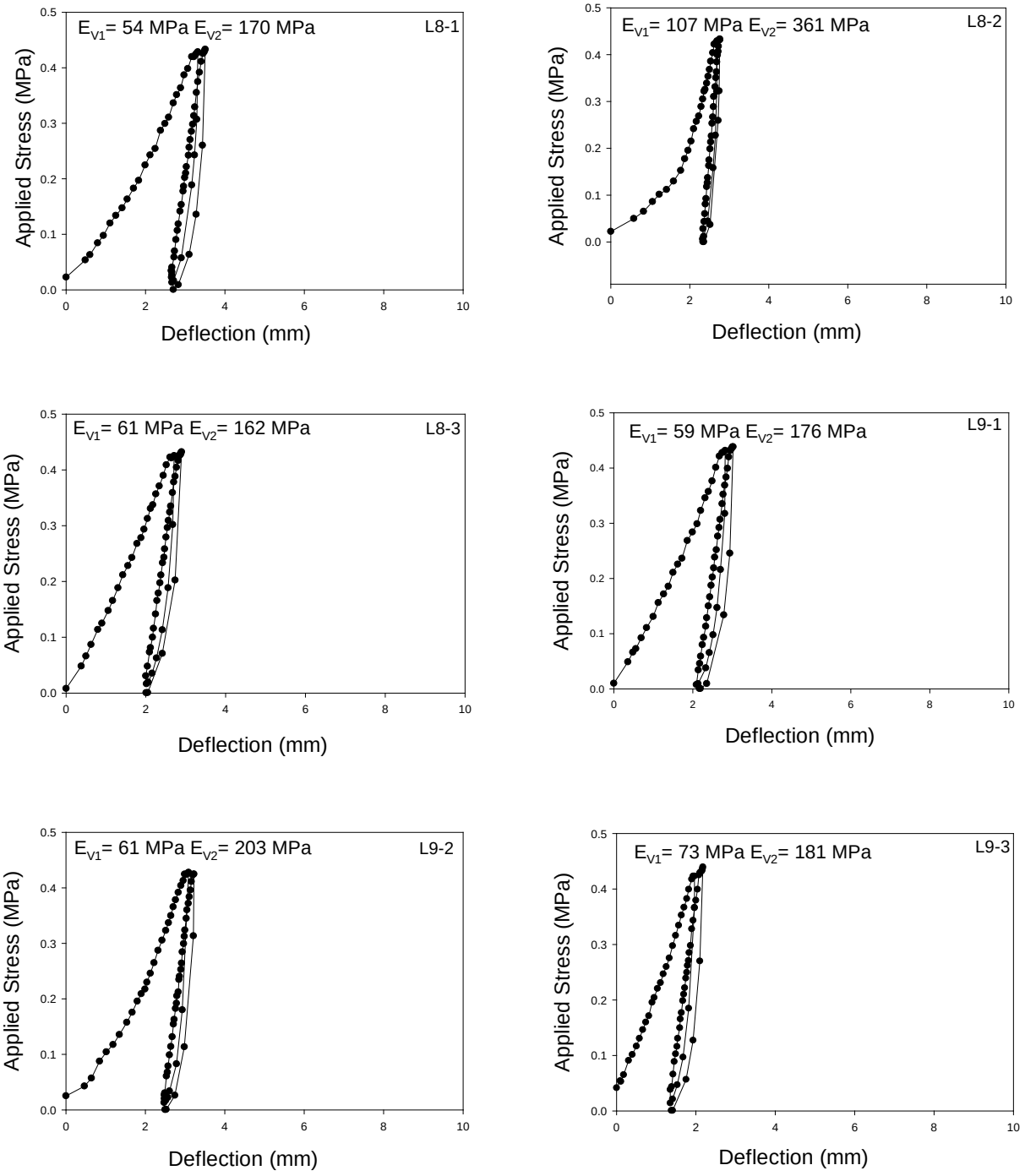

Figure 55. TB2: Stress-strain curves after low amplitude vibratory compaction (8, 9)

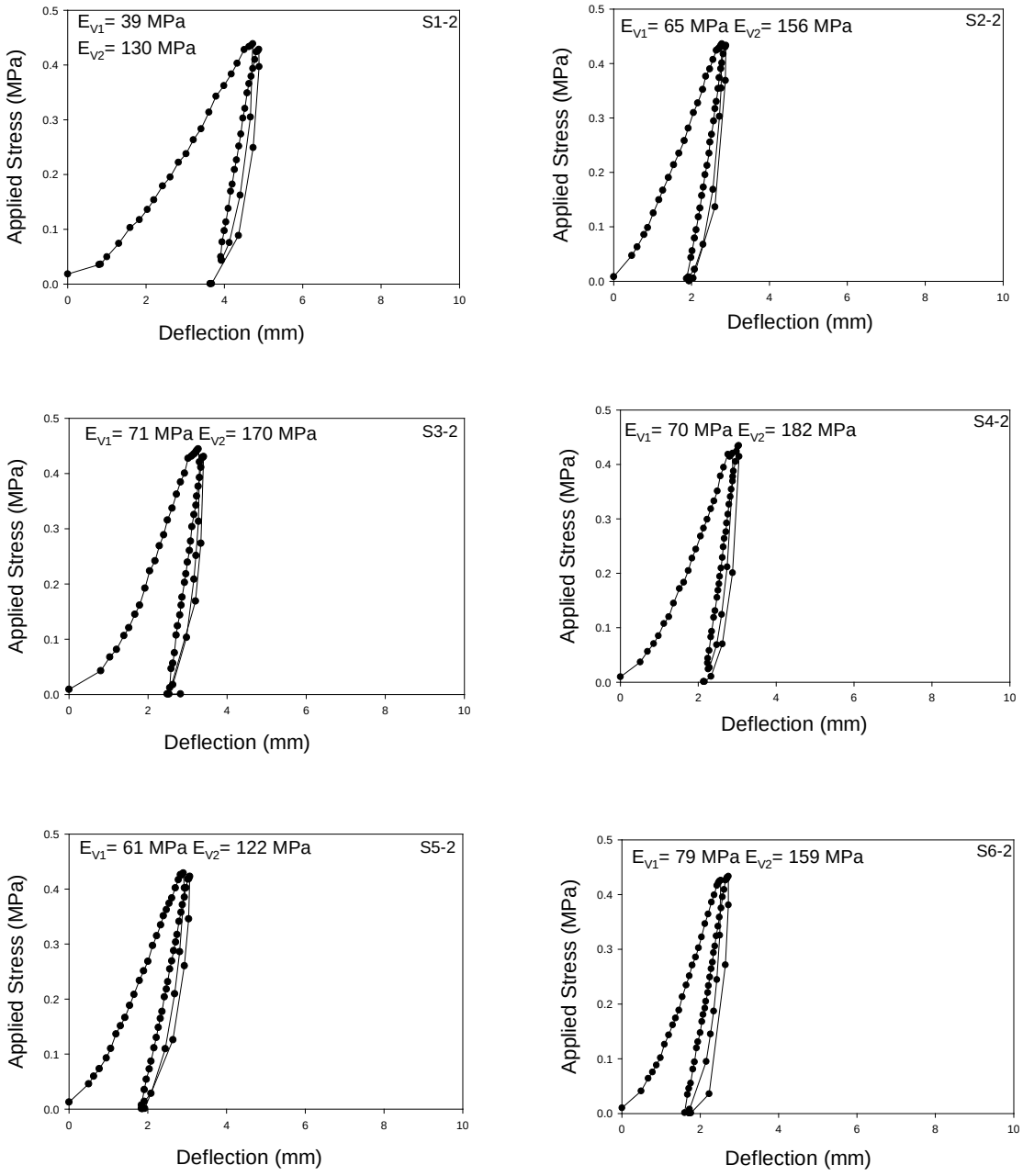

Figure 56. TB2: Stress-strain curves after low amplitude vibratory compaction (1, 6)

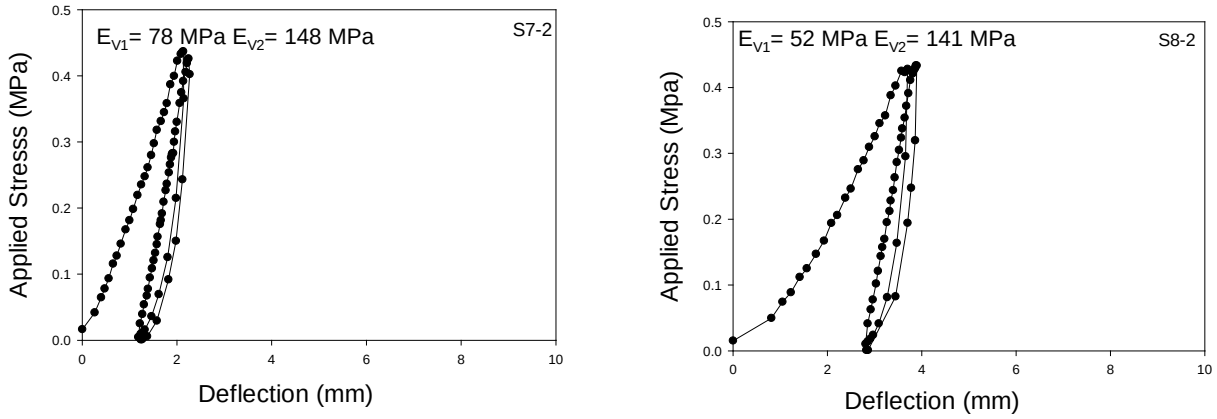

Figure 57. TB2: Stress-strain curves after low amplitude vibratory compaction (7, 8)